Investigating the Acoustic Response and Contrast Enhancement of Drug Loadable PLGA Microparticles with Various Shapes and Morphologies

Ipshita Gupta[†], Xiaoqian Su[†], Umesh Sai Jonnalagadda[†], Dhiman Das[†], Manojit Pramanik[†], and James J. Kwan*[†‡]

[†]School of Chemical and Biomedical Engineering, Nanyang Technological University, Singapore, 637459

*Corresponding Author
Dr. James Kwan
Associate Professor
Department of Engineering Science
University of Oxford, UK, OX1 3PJ
Email: james.kwan@eng.ox.ac.uk

[‡]Present Address: Department of Engineering Science, University of Oxford, United Kingdom, OX1 3PJ

Abstract:

Polymer nanoparticles and microparticles have been primarily used for drug delivery. There is a now a growing interest to further develop polymer-based solid cavitation agents to also enhance ultrasound imaging. We previously reported on a facile method to produce hollow poly(lactic-co-glycolic acid) (PLGA) microparticles with different diameters and degree of porosity. Here, we investigate the cavitation response from these PLGA microparticles with both therapeutic and diagnostic ultrasound transducers. Interestingly, all formulations exhibited stable cavitation; larger porous and multicavity particles also provided inertial cavitation at elevated acoustic pressure amplitudes. These larger particles also achieved contrast enhancement comparable to commercially available ultrasound contrast agents with a maximum recorded contrast-to-tissue ratio of 28 dB. Therefore, we show that multi-cavity PLGA microparticles respond to both therapeutic and diagnostic ultrasound, and may applied as a theranostic agent.

Keywords:

Therapeutic ultrasound, Diagnostic ultrasound, Theranostic agent, ultrasound imaging contrast agent, PLGA microparticles

Introduction

Conventional ultrasound contrast agents (UCAs) are gas filled microbubbles having a lipid or protein shell[Cosgrove 2006]. At low pressure amplitudes, UCAs undergo linear oscillations often referred to as stable or non-inertial cavitation[Calliada, et al. 1998]. The scattered sound from stable cavitation is often used in diagnostic imaging to create specific contrast imaging modes such as subharmonic imaging, harmonic imaging, and superharmonic imaging[Forsberg, et al. 2005]. Stable cavitation also perturbs the surrounding fluid to create microstreams that facilitates drug transport [Burgess, et al. 2015, Choi, et al. 2010, Mitragotri 2017, N. (2016), Zhou, et al. 2019]. At greater pressure amplitudes, UCAs begin to oscillate nonlinearly[Cosgrove 2006]. Above a critical pressure amplitude for a given bubble size and driving frequency the dynamics of the bubble becomes governed by the inertia of the surrounding fluid, i.e., inertial cavitation[Leighton 1994, Stride and Coussios 2019].This bubble motion is dynamic, exhibiting both arrested bubble motion and violent collapses of the microbubble that generate shock waves[Ohl, et al. 2015], fluid jets[Chen, et al. 2011], and fragmentation into smaller bubbles[Azmin, et al. , Chen, et al. 2003]. Several bioeffects, including tissue ablation [Tran, et al. 2003], sonoporation [Piotr Wawryka, et al. 2019], and tissue homogenization [Parsons, et al. 2006] have been attributed to the intense physical effects of inertial cavitation.

Generally it is desirable for UCAs to be monodispersed in diameter within a size range from 1-5 μm and sustain cavitation for extended periods of time[Song, et al. 2018]. The reason for this is twofold. firstly, there is a risk of serious complications such as embolism with oversized microbubbles, secondly, monodispersed bubbles provide a homogenous and higher echogenicity as both the resonance frequency for imaging and trigger frequency for therapy with ultrasound are size-dependent [Gong, et al. 2010, Zhang, et al. 2016]. Therefore, monodispersity is a critical measure for ultrasound contrast agent development

However, commercial lipid-shelled UCAs are typically polydisperse and suffer from limited stability due to coalescence and dissolution of the gas core leading to a short half-life (<10 min)[Mullin, et al. 2011, Yang, et al. 2013]. To overcome these limitations, there continues to be intense efforts in

designing and engineering fit-for-purpose UCAs. For example, solid cavitation agents [Chen, et al. 2017, Kwan, et al. 2015, Manzano and Vallet-Regí 2019, Su, et al. 2019, Thomas, et al. 2019] and non-lipid materials for the shell of microbubbles have been explored [Cui, et al. 2005, Larsson, et al. 2013, Lin, et al. 2009, Park, et al. 2012, Song, et al. 2018]. Unlike commercial UCAs that stabilise gas microbubbles by reducing the surface tension with a shell, solid cavitation agents entrap bubbles on hydrophobic surface cavities. In doing so, solid micro- and nanoparticles with surface-trapped bubbles have an exhibited extended circulation half-life and provide sustained cavitation for several minutes as these solid particles do not get destroyed by cavitation [Stride and Coussios 2019]. Yet, a majority of these solid cavitation agents are non-degradable [Thomas, et al. 2019].

In the context of solid cavitation agents, the cavitation threshold for these particles is defined by the peak negative pressure of the acoustic wave necessary to produce acoustically detectable noise from bubbles trapped on the surface or within the solid particle. Interestingly, many of the previously reported solid cavitation agents such as mesoporous silica nanoparticles [Yildirim, et al. 2013], gold nanocones [Mannaris, et al. 2018] and polystyrene nanocups [Kwan, et al. 2015] emitted only broadband noise in response to ultrasound, suggesting the occurrence of only inertial cavitation. This noise originates from the volumetric oscillation or inertial collapse of the gas bubble either pinned to, or detached from, the solid. This bubble motion is resisted by the inertia and viscosity of the surrounding medium and the surface tension of the bubble; the cavitation threshold of the solid cavitation agent are therefore dependent on the acoustic frequency. Generally, cavitation threshold is linearly related with both frequency and size of the cavitation agent [Holland and Apfel 1999]. Lower frequencies provide slower rates of bubble expansion and compression, minimizing inertial and viscous resistance compared to higher frequencies. Therefore as expected, solid cavitation agents have lower cavitation thresholds at lower frequencies [Kwan, et al. 2015]. In contrast, smaller cavitation agents require higher pressure amplitudes to nucleate cavitation, owing to the need to overcome the Laplace pressure of the gas bubble [Holland and Apfel 1989]. Size, shape, and acoustic frequency therefore play a crucial role in determining the acoustic response of solid cavitation agents, and subsequently their utility as a diagnostic and/or therapeutic agent.

Our group has previously reported on an "all-in-one" drug-loadable multi-cavity solid cavitation agent comprised of polylactic-co-glycolic acid (PLGA) [Su, et al. 2020, Su, et al. 2019], an FDA approved polymer known for its hydrolytic degradation and biocompatibility [Makadia and Siegel 2011, Su, et al. 2019]. However, their potential as an UCA and the effect of cavity density (or porosity) on the acoustic response of these microparticles remain unknown. We therefore investigated the acoustic response and contrast enhancement of PLGA microparticles with varying shapes and morphologies using both therapeutic and diagnostic ultrasound transducers. Considering the reduced cavitation thresholds and increased contrast enhancement, exotically shaped PLGA microparticles may be used as a theranostic agent.

Materials and Methods

Materials and reagents

Poly(lactide-co-glycolide 50:50) (PLGA, ResomerRG504 H), Poly(vinyl alco- hol) (PVA) (Mw 9,000–10,000, 80% hydrolyzed), Dichloromethane (anhydrous, > = 99.8%), Rhodamine B, Phosphate buffered saline (PBS) was purchased from Sigma-Aldrich, Singapore and used as received. Agarose was bought from Vivantis Technologies, Selangor Darul Ehsan, Malaysia. Deionized water was obtained from a pure water system (Stakpure, Niederahr, Germany). All sample chambers and HIFU transducer holders were built in house.

Preparation of PLGA particles

PLGA nanoparticles were prepared as described previously [Su, et al. 2020]. 50 mg of PLGA and 0.5 mg of RhB was dissolved in 2 mL of dichloromethane (DCM). Then 100 µl of PBS was added to the organic mixture and sonicated (Ultrasonic processor VCX 130, Sonics and Materials Inc.,Newtown, CT, USA) at 100 W for 30 s in an ice bath to form an emulsion. The obtained water-in-oil (W/O) emulsion was poured into a PVA solution and homogenized over ice for 5 min. Then this particle suspension was stirred for 3 h in a chemical fume hood to allow organic solvent evaporation. The PLGA particles were collected by centrifugation at 1,000 G for 5 min, after which they were

redispersed and washed three times with distilled water. After the final wash, the microparticles were freeze dried (Alpha 2-4 LSCbasic, Christ, Germany) for 48 h to achieve a dried powder for long term storage. The formulations investigated were 0x, 1x, 5x, and 10x PBS, and 1%, 3%, 5%, and 10% PVA. 1x PBS is given as 0.01 M concentration in accordance to the manufacture instructions [Su, et al. 2019].

Characterization of microparticles

Size and surface morphology of RhB-PLGA were assessed using a JEOL JSM-6700 Field Emission Scanning Electron Microscope (FE-SEM; JEOL Ltd., Akishima, Tokyo, Japan) at an acceleration voltage of 5 kV. Samples for the SEM were prepared by dropping 10 µl of 1 mg/ml suspension on silica wafers and air drying. The wafers were mounted onto a metal stub using double-sided electrical tape and coated with platinum (JFC 1600 Auto Fine Coater, JEOL Ltd., Akishima, Tokyo, Japan) for 2 min at 20 mA. All images were recorded under Secondary Electron Imaging (SEI) mode. Size distributions were determined by dynamic light scattering (DLS) (Malvern Nano-ZS, Malvern Panalytical, Malvern, UK).

Sample Holder

To make the acoustically transparent agarose sample chamber, 1% (w/v) of agarose solution was boiled and degassed for 30 min. The agarose solution was then poured into a bespoke cuboid mould (50 mm in length × 30 mm in width) and sealed with acoustically transparent mylar windows. A 1.6 mm steel rod was threaded through the mould. The rod was removed after gelation was complete, creating a channel for fluid flow.

Resuspension of microparticles

The dry powder was resuspended by mixing with deionized water and vortexed briefly (<5 sec) which led to no agglomeration as indicated by a the polydispersity index (PDI) = 0.13 by DLS. The particles were pumped into the acoustic sampling window and the containment vessel and no sedimentation was

observed for particle diameters < 5 µm. For larger variants, i.e. diameter > 5 µm , sedimentation was observed after 10 min. To prevent this, all experiments were completed within 7 minutes.

Therapeutic ultrasound setup

A 1.1 MHz high intensity focused ultrasound (HIFU) transducer (H102, Sonic Concepts, Bothell, WA, USA) was used for acoustic excitation. A 15 MHz passive cavitation detector (PCD) (V319, Olympus, Singapore) - co-axially aligned with the HIFU transducer focus - was used for detection of acoustic emissions at the HIFU focus. The HIFU transducer was calibrated using a 0.2 mm needle hydrophone (SN2562, Precision Acoustics, Dorset, UK). The geometric focus of the transducer was 1.37 mm in width and 10.21 mm in length. The HIFU transducer was driven by a function generator (33210 A, Keysight Technologies, Santa Rosa, CA, USA) and a RF power amplifier (1040 L, Electronics & Innovation, Rochester, NY, USA). All experiments with HIFU were carried out in a large tank filled with filtered, degassed, and deionized water. Acoustic amplitudes in this study were reported in MPa peak negative pressure amplitudes. A schematic representation of the setup is shown in figure 1.

Acoustic characterization of microparticles

The agarose phantom was submerged in the degassed water tank and aligned to the focus of the transducer. With the channel filled with air, the PCD was driven with a pulser-receiver (JSR Ultrasonics DPR300, Imaginant, Pittsford, NY, USA) to determine the position of the channel. A 3D positioning system was used to adjust the chamber until the channel was at the focus of the HIFU transducer. A 1 mg/ml suspension of microparticles were flowed through the channel using a syringe pump at a rate of 0.2 ml/min for ultrasound exposures. PLGA microparticles were exposed to 20 cycle bursts with increasing peak negative pressure amplitude at a pulse repetition period of 0.1 s. Acoustic emissions from PLGA microparticles were detected using a 15 MHz PCD co-axially aligned with the HIFU transducer. The PCD output was amplified using a broadband preamplifier (SR445A, Stanford Research Systems, Sunnyvale, CA, USA). The received signals were then recorded onto an oscilloscope

(DXOX3032A, Keysight Technologies, Santa Rosa, CA, USA) and post processed to determine the power spectral density (PSD) curve. For each burst, the area under the PSD curve was determined and compared to degassed water exposed to HIFU under the same conditions. Following the signal processing using MATLAB R2019b (MathWorks, Natick, MA, USA) cavitation was considered to have occurred if the received signals were 6 dB higher than noise from the water control [Kwan, et al. 2015, Kwan, et al.]. The probability of cavitation was determined as the percentage of bursts that recorded a cavitation event out of the total number of HIFU bursts (120 bursts).

Cavitation Threshold Determination

To estimate the cavitation threshold, a sigmoid function was fit to the probability for both harmonic and broadband signal. The sigmoid fitting function is defined in eq. 1:

$$f = \frac{1}{1+e^{-((p-p_{50})k)}} \qquad \ldots\ldots (1)$$

Where, f is the probability for cavitation, p is the input pressure, p_{50} is the cavitation threshold defined as the pressure amplitude value for achieving in 50% of the total number of pulses contained a cavitation, k is the slope of the fit. This function was fit to the experimental data by minimising the sum of square residuals using Microsoft Excel (Microsoft Corporation, Redmond, WA, USA).

Diagnostic Acoustic Setup

An E-Cube 12-R (Alpinion Medical Systems, Seoul, South Korea) clinical ultrasound imaging system with a linear array transducer (L3-12, Alpinion Medical Systems, Seoul, South Korea) was used to acquire images at the focal zone depth (5 cm) at a 12 Hz framerate. Scanning was performed with B mode operating at 10 MHz. Additionally, the mechanical index of this scanner was 1.1 at a 100% acoustic power giving a peak negative pressure of 3.2 MPa [Holland and Apfel 1999]. Data was saved in triplicate for each sample. Three independent samples for each formulation were tested. A schematic representation of the diagnostic ultrasound setup is shown in figure 2.a.

Contrast enhancement

For contrast enhancement measurements, a flow system was implemented using an acrylic water bath, a syringe pump (KD Scientific, Holliston, MA, USA), and flexible low-density polyethylene tubes (outer diameter 2.42 mm, thickness 0.37 mm). A dose of 6 mL reconstituted PLGA particles (1 mg/ml) were infused into the phantom holder via a syringe pump at a constant rate of 1 ml/min. The sample holder was placed in a water bath and the probe was placed directly above the vessel. As a control, deionized water was also run through the sample chamber and saved. The data was saved in triplicate in B-Mode. Afterwards contrast to tissue ratio (CTR) analysis was performed using ImageJ 1.52q (National Institutes of Health, Bethesda, MD, USA) to quantify the ability of each PLGA particle sample to distinguish between vessel and tissue using eq 2: [Hill, et al. 1990]

$$CTR = \frac{2(\mu_t - \mu_v)^2}{(\sigma_t^2 - \sigma_v^2)^2} \quad \ldots. (2)$$

where μ_t and μ_v represent the mean backscatter signal strength in the tissue and within the vessel lumen region, respectively, while σ_t^2, and σ_v^2 represent the corresponding variances. Four region-of-interests (ROIs) within the tissue and two ROIs within the vessel were selected. Each ROI was a 0.5x0.5 mm square. Images were acquired in triplicate for each sample using the linear array probe. The mean signal was averaged across all tissue and vessel ROIs to reduce variability. The four tissue ROIs were selected along the same horizontal and vertical axes as the vessel ROIs (as shown in Figure 2.b)

Results

SEM images of PLGA microparticles (Figure 3) prepared using the double emulsion-diffusion-evaporation method exhibited a multitude of diameters and porosity proportional to the concentration of porosigen (PBS) and stabilizer (PVA) and have been labelled into 4 categories, details of which are provided in the following sections, based on their morphology and diameter namely a) non-porous hollow spheres, b) porous hollow spheres, c) large multicavity particles (> 5 μm in diameter), and d) small multicavity particles (<5 μm in diameter). For ease of understanding, we made an arbitrary

classification of the type of porous opening, i.e., either as pores which were holes running throughout the thickness or as cavities, which were surface indentations not running throughout the thickness of the shell but limited to the surface.

PLGA microparticle formulations without PBS in the internal aqueous phase led to nonporous hollow spheres irrespective of the quantity of stabiliser. As expected, increasing the amount of porosigen in the internal aqueous phase of the water-in-oil-in-water (W/O/W) droplet resulted in hollow spheres with small and infrequent pores. Further increases of PBS concentration led to multicavity particles that were not uniformly spherical. Instead, cup shapes, highly porous spheres, and various aspherical shapes were present. In contrast, increasing the amount of stabilizer present in the bulk aqueous phase prior to heating inhibited the presence of pores and decreased the diameter of the polymer particles for all formulations [Su, et al. 2020]. We recognize that the population of multicavity particles may have porous particles present and vice versa. Thus, these categories are based on the predominant observed structure. For this study, the multicavity particles were separated into two groups based on diameter, i.e., large multicavity particles (> 5 μm) and small multicavity particles (< 5 μm). This cut-off to distinguish the larger from the smaller variants at 5 μm was chosen so as to distinguish the multicavity particles and compare their acoustic response to both setups of HIFU and the diagnostic imaging and then determine their ideal potential use in the different ultrasound regimens. Smaller variants would be ideal for use in the therapeutic domain given their favourable size, and the larger particles would nucleate bubbles with a larger scattering cross section and behave as better contrast agents but achieve poorer perfusion. Another reason for this distinction at 5 μm was to allow for a direct comparison between the contrast enhancement from the smaller microparticles and from the majority of the commercially available UCAs, all of which are all less than 5 μm in diameter on average[David E Goertz, et al. 2007, PC. 2008, Schneider 1999], and to determine if the larger diameter microparticles performed differently

Cavitation Response

Figure 4 shows representative images of normalized PSD curves for three different shapes of particles, namely the hollow spheres, small multicavity, and large multicavity microparticles. Cavitation was detected for all types of microparticles. Although the presence of harmonic emissions was observed for all microparticle formulations, substantial broadband emissions were only present for some of the formulations and was dependent on both the diameter of the microparticle and acoustic intensity (Figure A1). Broadband emissions, if present, only became apparent at pressure amplitudes larger than the pressure amplitudes required for harmonic emissions.

Figure 5 shows the estimated harmonic and broadband cavitation thresholds determined by the probability of cavitation (Figure A2) for all the microparticles tested. Both harmonic and broadband thresholds were governed by the diameter and shape of the microparticles. Irrespective of shape, larger microparticles had lower cavitation thresholds. This trend was most evident for the onset of broadband noise. Regarding the shape of the microparticles, there was generally a lower cavitation threshold for both harmonic and broadband emissions for porous particles compared to smooth hollow spheres. Similarly, more porous particles, i.e., multicavity microparticles as opposed to surface pores on spheres, emitted harmonic and broadband noise at lower input pressures; larger cavities nucleated cavitation at the lowest acoustic intensity.

Contrast Enhancement

The representative images for all the microparticle formulation samples tested with the diagnostic ultrasound setup at maximum input power, along with their calculated CTR values are shown in Figure 6. Generally, smaller and smoother microparticles had lower CTR values compared to more porous particles. The highest CTR values corresponded with larger multicavity particles (5.12 µm to 5.18 µm in diameter).

Figure 7 shows the measured CTR for representative microparticles from the different morphology groups (2 µm in diameter smooth spheres, 2 µm in diameter multicavity microparticles, and 6 µm in diameter multicavity microparticles) in addition to deionized water for increasing input pressures from 10% to 100% power (corresponding MI values of 0.11 to 1.1). The CTR of the 2 µm in

diameter smooth spheres remained at 6 dB for all input powers tested. Smaller multicavity microparticles provided CTR values greater than the smooth spheres at all input powers and displayed a subtle increase in CTR for input powers greater that 40%. Larger multicavity microparticles consistently delivered the highest CTR values for all powers tested. Similar to the smaller multicavity particles but to a greater extent, the CTR of the larger multicavity particles increased with increasing input power.

Discussion & Conclusion

In this study, we used a previously described method for making PLGA microparticles with a broad range of sizes and shapes[Su, et al. 2020]. The shapes formulated were hollow nonporous spheres (or simply polymer shelled microbubbles), porous spheres, and multicavity particles with surface indentations.

Hollow sphere or shelled microparticles are an established category of microparticles. With a gaseous core, these polymer shelled microbubbles have been extensively studies for both diagnostic and therapeutic application. They are of interest because of their ability to encapsulate water soluble drugs such as small molecular therapeutics and proteins[Ansary, et al. 2017, Cohen-Sela, et al. 2009]. The porous and multi-cavity particles are of interest as they tend to have larger surface area to volume ratios compared to smooth spheres, resulting in faster degradation[Klose, et al. 2006]. The surface cavities also trap gas, which may enable ultrasound-responsiveness[Straub, et al. 2005]. In this study, PBS in the internal aqueous phase was used as a porosigen to produce surface cavities and pores throughout the shell of the microparticle. The pores and cavities originated from water transport from the outer aqueous phase towards the inner aqueous phase due to the osmotic pressure gradient. As water attempts to transit the organic phase, phase separation occurs causing aqueous droplets on the surface and throughout the organic phase to form. These droplets then become the surface cavities and pores found on the final microparticle.

It is well known that the osmotic pressure from the addition of PBS in the aqueous core will cause swelling. This swelling resulted in larger diameters of the final microparticles. To mitigate

swelling, we added PVA into the bulk aqueous phase to prevent coalescence of the water droplets and maintain the stability of the W/O/W emulsion[Su, et al. 2020]. As expected, we observed that the addition of PVA reduced the size of the microparticle regardless of the salt concentration.

Unexpectedly, all PLGA microparticle formulations tested emitted detectable harmonic noise in response to therapeutic ultrasound, indicative of stable cavitation. This observation was in contrast to previously studied solid cavitation nuclei such as polystyrene nano-cups and gold nano-cones, which emitted only inertial cavitation[Kwan, et al. 2015, Mannaris, et al. 2018]. One explanation for this discrepancy is that the presence of multiple large pores and cavities on PLGA porous and multicavity particles trap numerous gas bubbles on the surface, which expand during the negative cycle of the ultrasound pulse. Since the pores are neighboring each other, the individual gas bubbles may possibly coalesce due to the proximity to form larger bubbles capable of both stable and inertial cavitation. It can also be seen from figure A2, that as the size decreased for each morphology group, a higher input pressure was required to achieve 50% probability of harmonic cavitation. This observation was likely because smaller cavities which extrude smaller bubbles require a higher input pressure to nucleate cavitation [Neppiras and Noltingk 1951]. The presence of stable cavitation from our PLGA microparticles at clinically relevant diameters suggests the potential for these microparticles to be used for imaging in various modes including harmonic and potentially even for subharmonic imaging. Beyond ultrasound contrast enhancement, stable cavitation also plays an important role in drug delivery. For example, stable cavitation has been attributed to as enhanced microstreaming for micromixing [Jordens, et al. 2016], drug delivery to tissue and cells[Tzu-Yin, et al. 2013], and reversible permeation of membranes such as the blood−brain barrier[Choi, et al. 2010]. Thus, presence of stable cavitation from all formulations is a critical and novel observation for our particles, potentially making them useful for imaging and drug delivery.

In the pressure amplitudes tested with multicavity and porous microparticles, considerable broadband noise at the higher acoustic pressure amplitudes was recorded for the larger particles in these two groups. The lack of inertial cavitation for some of the smaller porous and multicavity particles, as seen in figure A2, may be explained by their higher inertial threshold as seen in figure 3. One reason for the high threshold is the smaller initial diameter of the gas bubbles that were pulled from these

particles, where the surface tension prevented them from the initial sudden expansion and thus inertial cavitation did not occur at the pressures that were tested[Leighton 1994]. While considering the use of these particles for inertial cavitation bioeffects, the choice of target location will govern the type of formulation employed. The larger multicavity particles, given their size will be limited to blood vessels as they cannot extravasate into the capillary structures which require particles less than 2 μm[Zhao, et al. 2013]. However, the smaller multicavity particles and the porous spheres can be used for the micro-capillary structures as they are within the clinically relevant size (< 2 μm).

Also, we were unable to detect consistent broadband noise from hollow spheres at any pressure amplitude tests. This lack of broadband noise from the hollow spheres may be due to the much higher pressures required to inertially cavitate the hollow spheres. As can be seen in figure 5, for a similar particle size, the hollow spheres had the highest pressure threshold, followed by the porous spheres, with the lowest threshold for the multicavity particles. Considering that for hollow spheres the gas is trapped within a fully intact shell, inertial cavitation only occurs after the polymer shell is destroyed by the expansion of the bubble. Therefore, the shell properties will have a direct influence on the inertial cavitation threshold; generally, rigid polymer shelled bubbles will require a larger pressure amplitude to initiate inertial cavitation compared to lipid and surfactant-free gas bubbles[Church 1995, Paefgen, et al. 2015]. This phenomenon was also corroborated by Dicker et al. who reported the inertial thresholds for a microbubble sample encapsulated by a monolayer made with 95% gel phase lipid. They showed that the percentage of sample destroyed at 1 MPa peak negative pressure reduced from 70% to 20% when the sample was nested within a polymer shell[Dicker, et al. 2011]. Our results for the inertial cavitation threshold for the hollow spheres indicated that a pressure range between 4.5 MPa to 9 MPa was required to achieve 50% probability of inertial cavitation. These results are higher than previously reported threshold values by Wallace et.al who reported a pressure threshold ranging between 1.5 to 2 MPa for microbubbles nested in a polymer shell with a 2.5 MHz transducer. However, the discrepancy can be accounted for by the different production methods of the microparticles and the different transducer frequency employed. The interplay between Laplace pressure, contact angle, and the size of crevice and the corresponding nucleated bubble may provide a better understanding of this phenomenon

[Apfel 1970, Atchley and Prosperetti 1989, Yildirim, et al. 2016]. Laplace pressure, is defined as $2\sigma R^{-1}$ (by neglecting the ambient pressure), where σ is the surface tension of water and R is the radius of curvature of the liquid-gas interface[Atchley and Prosperetti 1989]. Unlike spherical bubbles, which have positive curvature, i.e. the radius of curvature lies towards the gas side of the interface, solid cavitation nuclei have crevices with trapped bubbles. These surface trapped bubbles have a negative curvature, making the trapped bubble highly stable[Yildirim, et al. 2016]. The contact angle α is the angle measured in the liquid, which the liquid-gas interface makes with the solid. It must satisfy the relationship $\alpha_r < \alpha < \alpha_a$, where α_r is the receding contact angle, i.e., the limiting angle the liquid gas interface makes with the solid during receding after initial wetting, and α_a is the advancing contact angle, i.e., the angle at which the liquid-gas interface will advance along the solid crevice wall and cause during nucleation[Apfel 1970]. As per Atchley et al. the nucleation threshold is the value of liquid pressure at which the contact angle reaches the receding value[Atchley and Prosperetti 1989]. At this value, any interfacial movement reduces both the curvature, thereby reducing the Laplace pressure and also the internal gas pressure. If the Laplace pressure reduces more rapidly, the system becomes unstable and rapid growth of the trapped bubble is observed. Apfel presented a theory where in crevices smaller than the critical size, a linear relationship between nucleation threshold and surface tension was observed, whereas no such relationship was observed for the larger crevices[Apfel 1970].

Non-porous hollow spheres are independent of surface tension and effect of crevice size and as expected, in figure 5a, their stable cavitation threshold does not show a strong linear relationship with particle diameter. In terms of inertial cavitation threshold, for the non-porous spheres, this is the acoustic pressure required to rupture the polymer shell. Figure 5 also suggests a strong linear relationship between cavitation threshold and particle diameter for all formulations of porous and multicavity particles, the most prominent for the porous samples. For stable cavitation threshold, this may be indicative of an effect of crevice size being lower than Apfel's description of critical crevice size, which has an effect on the contact angle and consequently on the nucleation threshold and subsequent stable cavitation. The R^{-1} dependence of inertial cavitation threshold for these three formulations in figure 5b may be a function of bubble size; smaller bubbles need higher pressures to rupture and overcome their Laplace pressure.

The presence of stable cavitation from our PLGA microparticles suggested the potential for these microparticles to be used for imaging. While testing for contrast enhancement with a diagnostic scanner, all particles gave a CTR higher than deionized water. The larger multicavity particles (> 5 μm) gave the highest enhancement, which agrees with the now established observation that larger particles with more cavities nucleate cavitation more easily and have a larger backscattered intensity. However, their size prevents these larger particles from being useful in several applications where penetration into the micro-capillary structure is required such as in hepatic tumors [Tang, et al. 2013], and prostate cancer[Cheng, et al. 2007] The clinically relevant particle sizes (diameter < 2 μm) gave a CTR of 21.86 dB. These particles achieved enhancement comparable to the commercially available ultrasound contrast agents [Gupta, et al. 2018, Lyshchik 2019, Paefgen, et al. 2015](CTR values 10-20 dB making them a good candidate for quicker clinical adoption). Although a high CTR was recorded for the larger porous and multicavity particles, the nonporous hollow spherical variants suffered from poor enhancement. This is in agreement with figure A1, where it is evident that the larger porous and muticavity particles emit significantly higher harmonic emissions as compared to the nonporous spherical variants. From figure A2, it is also clear that these spherical particles have a higher threshold for input pressures to achieve 50% probability of cavitation. Hence, it could be that the diagnostic pressures employed for this study were below the threshold for the hollow spheres and majority of particles did not achieve stable cavitation, thus giving a reduced enhancement as compared to the larger porous and multicavity particles. Optimizing the input pulse shape might also enhance the signal from these formulations. A previous study by Sciallero et al. indicates that changing the input pulse shape can enhance the echogenicity of these microparticles even more. They developed dual function PLGA shelled microbubbles with an average external diameter of 3.8 μm and showed that a chirp pulse provided a higher CTR as compared to the conventional pulse inversion method, achieving a CTR of 32 dB[Sciallero, et al. 2016].

Overall conventional UCAs have a poor drug encapsulation efficiency, suffer from polydispersity and have a short half-life, and previous polymer-based agents have shown a weak

capability in contrast imaging due to lack of stable cavitation and hence there are currently no FDA approved polymer shelled microbubbles[Paefgen, et al. 2015]. Here, we have successfully developed a PLGA based solid cavitation agent that overcomes this problem and establishes the use of these PLGA particles as imaging agents.

We next investigated the effect of increasing MI on contrast enhancement. Nonporous hollow spheres provided the least contrast enhancement and were comparable to the control sample of DI water. This observation may be explained by the fact that these solid microspheres have a rigid polymer shell and thus substantially higher cavitation thresholds than the porous and multicavity variants. The larger multicavity particles (> 5 μm) behaved differently than the smaller multicavity variants (< 5 μm). They showed a steep increase at 60% acoustic power beyond which they showcased a linear increase. This indicates that these particles have a threshold for input pressures beyond which their enhancement increases and hence must be optimized for each scanner being used for imaging. The smaller multicavity particles show no such trend and give similar enhancement for all input pressures which is also higher than the nonporous hollow spheres. One explanation for the nearly constant CTR values for the smaller (<5 μm) multicavity particles and up to a certain acoustic pressure for the larger (>5 μm) multicavity particles could be that these PLGA particles provide enhancement only due their nucleated bubbles. They have a scattering cross section (SCS) which is significantly lower than the bubbles which nucleate once the cavitation threshold is crossed. This implies that all the enhancement achieved is via the nucleated gas bubbles and negligible by the particles themselves. To help support this hypothesis we used the equation by Morse and Ingard [Moffett 1970] :

$$\sigma = \frac{4\pi}{9} k^4 r^6 \{[\frac{k_s - k}{k}]^2 + \frac{1}{3}[\frac{3(\rho_s - \rho)}{2\rho_s - \rho}]^2\} \quad \ldots\ldots\ldots (3)$$

Where σ is the SCS, k is the wave number, r is the radius, k and ρ are the compressibility and density, respectively, of the scatterer (subscripts) and the surrounding medium, i.e. deionized water. Using eqn. 3, if we assume the first part of the equation (before the curly brackets) to be a constant A, for gas bubbles, which have a very high compressibility (~ 2.3 x 10^{-4} cm^2/dyne) and very low density (~ 1.29 x 10^{-3} g/cm^3), we can assume, $k_s \gg k$ and $\rho_s \ll \rho$. Using these values, the SCS is on the order of 10^{14}

A cm^2 for the nucleated gas bubbles, ignoring any further resonance [Ophir and Parker 1989]. However, PLGA particles without any nucleated gas bubbles, have a compressibility (~ 0.5 x 10^{-10} cm^2/dyne) which is much lower than gas and very similar to the surrounding medium and density (~ 1.34 g/cm^3) which is much higher than gas and again similar to the surrounding water [Aldrich]. These values lead to a SCS values close to zero or very small as compared to the nucleated bubbles. Therefore, it is very likely that the smaller multicavity particles did not cross their higher threshold value and hence provided a linear response to the diagnostic ultrasound while the larger variants (> 5μm) achieved nucleation owing to their lower cavitation threshold and hence provided non-linear enhancement with increasing acoustic pressures.

In conclusion, we have successfully showcased the use of these "all-in-one" particles which can achieve targeted drug release, have surface cavities for sustained cavitation, have a tunable size and morphology, and also provide contrast enhancement comparable to commercial UCAs. By changing the size, morphology, and input acoustic pressure, we can exploit either the stable or the inertial cavitation response of these particles to achieve the desired mechanical effect. For use in therapy, the particles should ideally be less than 2 μm, respond to lower frequencies (therapeutic ultrasound range) and achieve sufficient cavitation to be able to penetrate the endothelium and release the drug in a sustained manner, in this case by natural biodegradation [Stride and Coussios 2019]. These can be achieved with majority of the non-porous, porous and the smaller multicavity (< 5 μm) particles as they all achieved stable cavitation. To exploit the mechanical effects of inertial cavitation in the therapeutic regimen such as for sonoporation, microjetting etc., the larger (~ 5 μm) porous and multicavity particles may be employed [Ohl, et al. 2015]. It should be noted that these particles, given their diameter will be restricted to remain in the blood flow as they cannot penetrate into the endothelium[Zhao, et al. 2013]. Next, for use as an ultrasound contrast agent, the particles should respond strongly, i.e. achieve sustained stable cavitation at the diagnostic ultrasound frequency range and scatter the ultrasound signal thereby providing a strong echogenicity[Paefgen, et al. 2015]. All multicavity particles (both large i.e. > 5 μm and small i.e. < 5 μm) may be used for this purpose. Given the larger size, the > 5 μm multicavity particles have a higher SCS for the nucleated bubbles and a lower

threshold to achieve stable cavitation and hence provide higher CTR(>20 dB). However, their size restricts them to remain in the blood vessels only. The smaller variants, i.e. <5 μm, achieve a lower CTR (~ 9 to 19 dB) however, these values are still comparable with the commercially used UCAs and their size allows them to extravasate into the endothelium for imaging of microcapillaries. Lastly, majority of the porous spherical variants and the smaller multicavity particles (<5 μm) prove to be most suitable for theranostic use such as ultrasound image guided therapy [Sun, et al. 2014]. Their size (~1.30 μm) which falls within the clinically relevant range and their acoustic response both to HIFU and diagnostic ultrasound with a CTR (7- 22 dB) comparable to current commercial UCAs makes them an ideal candidate for use as a theranostic agent.

Acknowledgements

The authors acknowledge the support from the Ministry of Education in Singapore under the Tier 1 grant scheme (RG144/18, RG127/19). This research is supported by the Singapore Ministry of Health's National Medical Research Council under its NMRC/OFYIRG/0034/2017. The authors have no relevant financial interests in the manuscript and no other potential conflicts of interest to disclose.

References

Aldrich MS. Resomer® RG 504 H, Poly(D,L-lactide-co-glycolide).

Ansary RH, Rahman MM, Mohamad N, Arrif TM, Latif AZA, Katas H, Nik W, Wan SB, Awang MB. Controlled Release of Lysozyme from Double-Walled Poly(Lactide-Co-Glycolide) (PLGA) Microspheres. Polymers 2017; 9:485.

Apfel RE. The Role of Impurities in Cavitation- Threshold Determination. The Journal of the Acoustical Society of America 1970; 48:1179-86.

Atchley AA, Prosperetti A. The crevice model of bubble nucleation. The Journal of the Acoustical Society of America 1989; 86:1065-84.

Azmin M, Harfield C, Ahmad Z, Edirisinghe M, Stride E. How do microbubbles and ultrasound interact? Basic physical, dynamic and engineering principles.

Burgess A, Shah K, Hough O, Hynynen K. Focused ultrasound-mediated drug delivery through the blood–brain barrier. Expert Rev. Neurother. 2015; 15:477-91.

Calliada F, Campani R, Bottinelli O, Bozzini A, Sommaruga MG. Ultrasound contrast agents: basic principles. Eur J Radiol. 1998

Chen F, Ma M, Wang J, Wang F, Chern S-X, Zhao ER, Jhunjhunwala A, Darmadi S, Chen H, Jokerst JV. Exosome-like silica nanoparticles: a novel ultrasound contrast agent for stem cell imaging. Nanoscale 2017; 9:402-11.

Chen H, Brayman AA, Kreider W, Bailey MR, Matula TJ. Observations of Translation and Jetting of Ultrasound-Activated Microbubbles in Mesenteric Microvessels. Ultrasound Med. Biol. 2011; 37:2139-48.

Chen WS, Matula TJ, Brayman AA, Crum LA. A comparison of the fragmentation thresholds and inertial cavitation doses of different ultrasound contrast agents. The Journal of the Acoustical Society of America 2003; 113:643-51.

Cheng J, Teply BA, Sherifi I, Sung J, Luther G, Gu FX, Levy-Nissenbaum E, Radovic-Moreno AF, Langer R, Farokhzad OC. Formulation of functionalized PLGA–PEG nanoparticles for in vivo targeted drug delivery. Biomaterials 2007; 28:869-76.

Choi JJ, Feshitan J, Baseri B, Wang S, Tung Y, Borden M, Konofagou EE. Microbubble-size dependence of focused ultrasound-induced blood-brain barrier opening in mice in vivo. IEEE transactions on bio-medical engineering 2010; 57(1):145-54.

Church CC. The effects of an elastic solid-surface layer on the radial pulsations of gas-bubbles. J. Acoust. Soc. Am. 1995; 97:1510-21.

Cohen-Sela E, Chorny M, Koroukhov N, Danenberg HD, Golomb G. A new double emulsion solvent diffusion technique for encapsulating hydrophilic molecules in PLGA nanoparticles. Journal of controlled release : official journal of the Controlled Release Society 2009; 133:90-95.

Cosgrove D. Ultrasound contrast agents: an overview. Eur. J. Radiol. 2006; 60(3):324-30.

Cui W, Bei J, Wang S, Zhi G, Zhao Y, Zhou X, Zhang H, Xu Y. Preparation and evaluation of poly(L - lactide- co - glycolide) (PLGA) microbubbles as a contrast agent for myocardial contrast echocardiography. Journal of Biomedical Materials Research Part B: Applied Biomaterials 2005; 73:171-78.

Goertz DE, de Jong N, van der Steen AFW. Attenuation and size distribution measurements of Definity and manipulated Definity populations. Ultrasound Med Biol. 2007; 33(9):1376-88.

Dicker S, Mleczko M, Hensel K, Bartolomeo A, Schmitz G, Wrenn SP. Coencapsulation of lipid microbubbles within polymer microcapsules for contrast applications. Bubble Science, Engineering & Technology 2011; 3:12-19.

Forsberg F, Liu JB, Shi WT, Furuse J, Shimizu M, Goldberg BB. In vivo pressure estimation using subharmonic contrast microbubble signals: Proof of concept. IEEE Trans Ultrason Ferroelectr Freq Control 2005; 52:581-83.

Gong Y, Cabodi M, Porter T. Relationship between size and frequency dependent attenuation of monodisperse populations of lipid coated microbubbles. Bubble Science, Engineering & Technology 2010; 2:41-47.

Gupta I, Eisenbrey JR, Machado P, Stanczak M, Wallace K, Forsberg F. On Factors Affecting Subharmonic-aided Pressure Estimation (SHAPE). Ultrason. Imaging 2018; 41:35-48.

Hill CR, Bamber JC, Cosgrove DO. Performance criteria for quantitative ultrasonology and image parameterization. Clin. Phys. Physiol. Meas. 1990; 11:57-73.
Holland CK, Apfel RE. An improved theory for the prediction of microcavitation thresholds. IEEE Transactions on Ultrasonics, Ferroelectrics, and Frequency Control 1989; 36:204-08.
Holland CK, Apfel RE. Fundamentals of the Mechanical Index and caveats in its application. The Journal of the Acoustical Society of America 1999; 105:1324-24.
Jordens J, Bamps B, Gielen B, Braeken L, Van Gerven T. The effects of ultrasound on micromixing. Ultrason. Sonochem. 2016; 32:68-78.
Klose D, Siepmann F, Elkharraz K, Krenzlin S, Siepmann J. How porosity and size affect the drug release mechanisms from PLGA-based microparticles. Int. J. Pharm. 2006; 314:198-206.
Kwan JJ, Graham S, Myers R, Carlisle R, Stride E, Coussios CC. Ultrasound-induced inertial cavitation from gas-stabilizing nanoparticles. Physical Review E 2015; 92:023019.
Kwan JJ, Myers R, Coviello CM, Graham SM, Shah AR, Stride E, Carlisle RC, Coussios CC. Ultrasound-propelled nanocups for drug delivery. Small (Weinheim an der Bergstrasse, Germany) 2015.
Larsson M, Larsson M, Oddo L, Margheritelli S, Paradossi G, Nowak J, Brodin L-A, Caidahl K, Bjallmark A. Visualization of multimodal polymer-shelled contrast agents using ultrasound contrast sequences: an experimental study in a tissue mimicking flow phantom.(Report). Cardiovasc. Ultrasound 2013; 11.
Leighton TG. 2 - Cavitation Inception and Fluid Dynamics, In: Leighton TG, ed. *The Acoustic Bubble*: Academic Press, 1994. 67-128.
Lin P-L, Eckersley RJ, Hall EAH. Ultrabubble: A Laminated Ultrasound Contrast Agent with Narrow Size Range. Advanced Materials 2009; 21:3949-52.
Lyshchik A. Specialty Imaging: Fundamentals of CEUS, 1st Edition: Elsevier, 2019.
Makadia HK, Siegel SJ. Poly Lactic-co-Glycolic Acid (PLGA) as Biodegradable Controlled Drug Delivery Carrier. Polymers 2011; 3:1377-97.
Mannaris C, Teo BM, Seth A, Bau L, Coussios C, Stride E. Gas-Stabilizing Gold Nanocones for Acoustically Mediated Drug Delivery. Advanced Healthcare Materials 2018; 7:1800184.
Manzano M, Vallet-Regí M. Ultrasound responsive mesoporous silica nanoparticles for biomedical applications. Chem. Commun. (Camb.) 2019; 55:2731-40.
Mitragotri S. Sonophoresis: Ultrasound-Mediated Transdermal Drug Delivery, In: Dragicevic N and I. Maibach H, eds. *Percutaneous Penetration Enhancers Physical Methods in Penetration Enhancement*. Berlin, Heidelberg: Springer Berlin Heidelberg, 2017. 3-14.
Moffett MB. Theoretical Acoustics. Science 1970; 170:156.
Mullin L, Gessner R, Kwan J, Kaya M, Borden MA, Dayton PA. Effect of anesthesia carrier gas on in vivo circulation times of ultrasound microbubble contrast agents in rats. Contrast Media Mol. Imaging 2011; 6:126-31.
Rapoport N. Drug-Loaded Perfluorocarbon Nanodroplets for Ultrasound-Mediated Drug Delivery. In: Escoffre JM., Bouakaz A. (eds) Therapeutic Ultrasound. Advances in Experimental Medicine and Biology: Springer, Cham, (2016).
Neppiras EA, Noltingk BE. Cavitation Produced by Ultrasonics: Theoretical Conditions for the Onset of Cavitation. Proceedings of the Physical Society. Section B 1951; 64:1032-38.
Ohl SW, Klaseboer E, Khoo BC. Bubbles with shock waves and ultrasound: a review. Interface focus 2015; 5:20150019-19.
Ophir J, Parker KJ. Contrast agents in diagnostic ultrasound. Ultrasound Med. Biol. 1989; 15:319-33.
Paefgen V, Doleschel D, Kiessling F. Evolution of contrast agents for ultrasound imaging and ultrasound-mediated drug delivery. Front. Pharmacol. 2015; 6:197.
Park Y, Luce AC, Whitaker RD, Amin B, Cabodi M, Nap RJ, Szleifer I, Cleveland RO, Nagy JO, Wong JY. Tunable diacetylene polymerized shell microbubbles as ultrasound contrast agents. Langmuir : the ACS journal of surfaces and colloids 2012; 28:3766.
Parsons JE, Cain CA, Abrams GD, Fowlkes JB. Pulsed cavitational ultrasound therapy for controlled tissue homogenization. Ultrasound Med. Biol. 2006; 32:115-29.
Sontum PC. Physicochemical characteristics of Sonazoid, a new contrast agent for ultrasound imaging. Ultrasound Med Biol. 2008; 34(5):824-33.

Wawryka P, Kiełbik A, Iwanek G. Microbubble based sonoporation — from the basics into clinical implications. Microbubble based sonoporation — from the basics into clinical implications 2019; 4:178-83-78-83.
Schneider M. Characteristics of SonoVue™. Echocardiography 1999; 16:743-46.
Sciallero C, Balbi L, Paradossi G, Trucco A. Magnetic resonance and ultrasound contrast imaging of polymer-shelled microbubbles loaded with iron oxide nanoparticles. Royal Society open science 2016; 3:160063-63.
Song R, Peng C, Xu X, Wang J, Yu M, Hou Y, Zou R, Yao S. Controllable Formation of Monodisperse Polymer Microbubbles as Ultrasound Contrast Agents. ACS Applied Materials & Interfaces 2018; 10:14312-20.
Song R, Peng C, Xu X, Wang J, Yu M, Hou Y, Zou R, Yao S. Controllable Formation of Monodisperse Polymer Microbubbles as Ultrasound Contrast Agents. ACS applied materials & interfaces 2018; 10:14312.
Straub JA, Chickering DE, Church CC, Shah B, Hanlon T, Bernstein H. Porous PLGA microparticles: AI-700, an intravenously administered ultrasound contrast agent for use in echocardiography. J. Control. Release 2005; 108(1):21-32.
Stride E, Coussios C. Nucleation, mapping and control of cavitation for drug delivery. Nature Reviews Physics 2019; 1:495-509.
Su X, Gupta I, Jonnalagadda U, Kwan J. Complementary Effects of Porosigen and Stabiliser on the Structure of Hollow Porous Poly(lactic-co-glycolic acid) Microparticles. ACS Applied Polymer Materials 2020.
Su X, Thomas RG, Bharatula LD, Kwan JJ. Remote targeted implantation of sound-sensitive biodegradable multi-cavity microparticles with focused ultrasound. Sci. Rep. 2019; 9:9612.
Sun Y, Wang Y, Niu C, Strohm EM, Zheng Y, Ran H, Huang R, Zhou D, Gong Y, Wang Z, Wang D, Kolios MC. Laser-Activatible PLGA Microparticles for Image-Guided Cancer Therapy In Vivo. Advanced Functional Materials 2014; 24:7674-80.
Tang L, Gabrielson NP, Uckun FM, Fan TM, Cheng J. Size-Dependent Tumor Penetration and in Vivo Efficacy of Monodisperse Drug–Silica Nanoconjugates. Mol. Pharm. 2013; 10:883-92.
Thomas RG, Jonnalagadda US, Kwan JJ. Biomedical Applications for Gas-Stabilizing Solid Cavitation Agents. Langmuir 2019; 35:10106-15.
Tran BC, Jongbum S, Hall TL, Fowlkes JB, Cain CA. Microbubble-enhanced cavitation for noninvasive ultrasound surgery. IEEE Transactions on Ultrasonics, Ferroelectrics, and Frequency Control 2003; 50:1296-304.
Tzu-Yin W, Katheryne EW, Steven M, Jurgen KW. Ultrasound and Microbubble Guided Drug Delivery: Mechanistic Understanding and Clinical Implications. Curr. Pharm. Biotechnol. 2013; 14:743-52.
Yang P, Ding J, Guo J, Shi W, Hu JJ, Wang C. A strategy for fabrication of uniform double-shell hollow microspheres as effective acoustic echo imaging contrast agents through a new polymer-backbone-transition method. Journal of Materials Chemistry B 2013; 1:544-51.
Yildirim A, Chattaraj R, Blum NT, Goodwin AP. Understanding Acoustic Cavitation Initiation by Porous Nanoparticles: Toward Nanoscale Agents for Ultrasound Imaging and Therapy. Chem. Mater. 2016; 28:5962-72.
Yildirim A, Demirel GB, Erdem R, Senturk B, Tekinay T, Bayindir M. Pluronic polymer capped biocompatible mesoporous silica nanocarriers. Chemical Communications 2013; 49:9782-84.
Zhang C, Wang Z, Wang C, Li X, Liu J, Xu M, Xu S, Xie X, Jiang Q, Wang W, Cao Z. Highly Uniform Perfluoropropane-Loaded Cerasomal Microbubbles As a Novel Ultrasound Contrast Agent. ACS Applied Materials & Interfaces 2016; 8:15024-32.
Zhao YZ, Du LN, Lu CT, Jin YG, Ge SP. Potential and problems in ultrasound-responsive drug delivery systems. International journal of nanomedicine 2013; 8:1621-33.
Zhou X, Guo L, Shi D, Duan S, Li J. Biocompatible Chitosan Nanobubbles for Ultrasound-Mediated Targeted Delivery of Doxorubicin. Nanoscale Research Letters 2019; 14:24.

Figure Captions

Figure 1: Schematic representation of the therapeutic ultrasound experimental setup.

Figure 2: a) Schematic representation of the diagnostic ultrasound experimental setup. b) Schematic for selection of region of interest (ROI) for vessel and tissue. CTR analysis was done by calculating the average of pixel intensity in the four tissue and two vessel ROIs selected. This was done to minimize variability.

Figure 3. SEM images of PLGA microparticles under different concentrations of PBS and PVA. The scale bar represents 1 um. The polydispersity index (PDI) ranged from 0.1 to 0.26. As can be seen, a wide variety of morphologies are produced depending on the amount of porosigen and stabiliser used. The samples were categorised into a) non-porous hollow spheres, b) hollow spheres with small and infrequent pores, c) large multicavity particles (> 5 μm; larger than commercially available UCAs), and d) small multicavity particles (< 5 μm; size comparable to commercial UCAs).

Figure 4. Representative images of the normalized spectral density curves for three different shapes of particles, namely the a) spherical and both the b) small and c) large multicavity particles. As is seen, the multicavity particles (see b & c) transitioned from stable to inertial cavitation at much lower pressures in comparison to the nonporous spherical variants.

Figure 5. Dependence of acoustic pressure amplitude required to achieve 50% probability of (a) harmonic and (b) broadband cavitation on the diameter of particles. The dependence on particle diameter can be observed indicating the effect of Laplace pressure on cavitation threshold most strikingly for the porous hollow spheres.

Figure 6. All samples as imaged with the diagnostic ultrasound scanner and the corresponding contrast to tissue ratio (CTR) values in dB with reference to deionized water. As is seen, highest enhancement (> 20 dB) was observed for the larger multicavity particles (diameter > 5μm) i.e., category (c): the right

top corner and in the sample in the middle of the matrix. These samples are highlighted in green. The control sample with deionized water is shown in the supplementary figure A3.

Figure 7. Contrast to tissue ratio (CTR) with respect to deionized water for hollow spheres, smaller and larger multicavity particles with increasing input acoustic power levels.

Figure

Click here to access/download;Figure;Figure 1.tiff

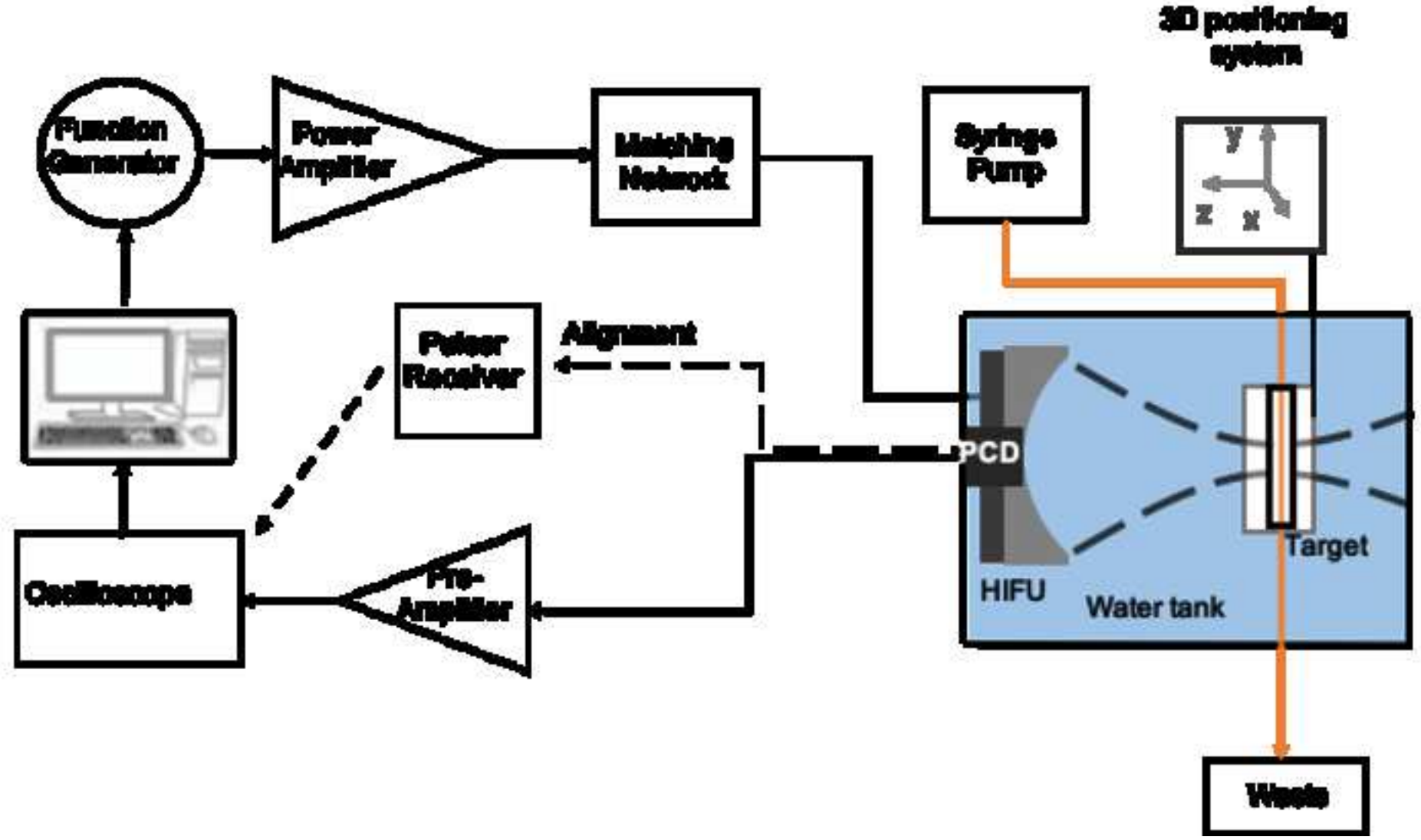

Figure

Click here to access/download;Figure;Figure 2.tiff

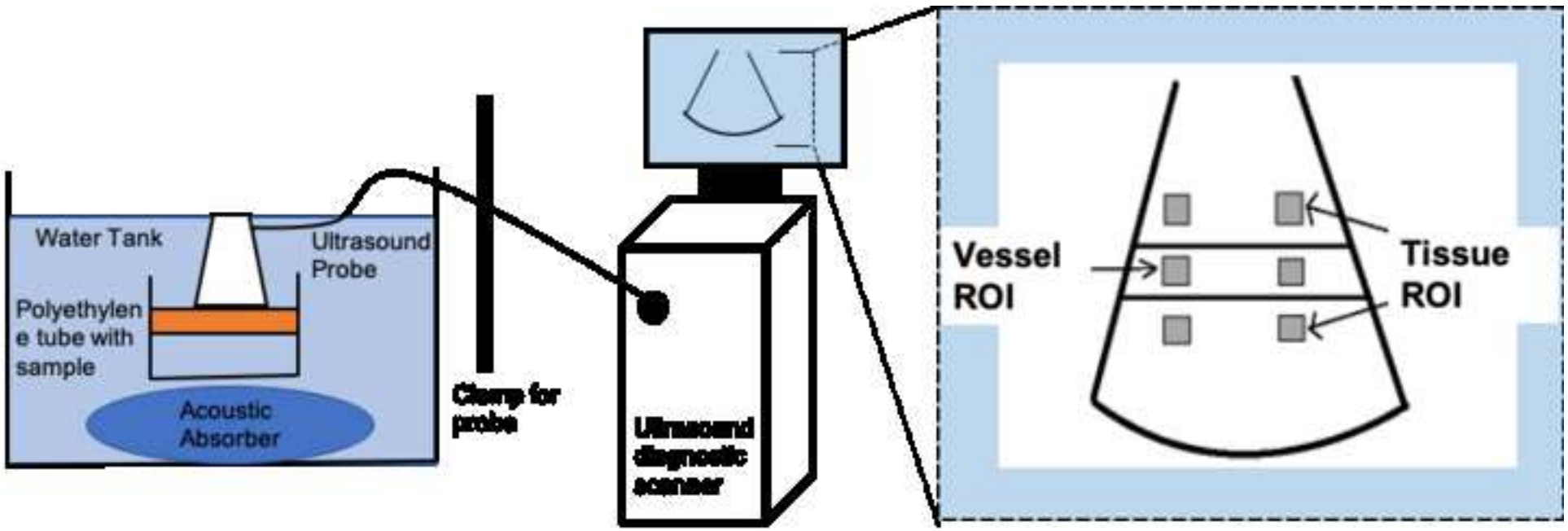

a b

Figure

Click here to access/download;Figure;Figure 3.tiff

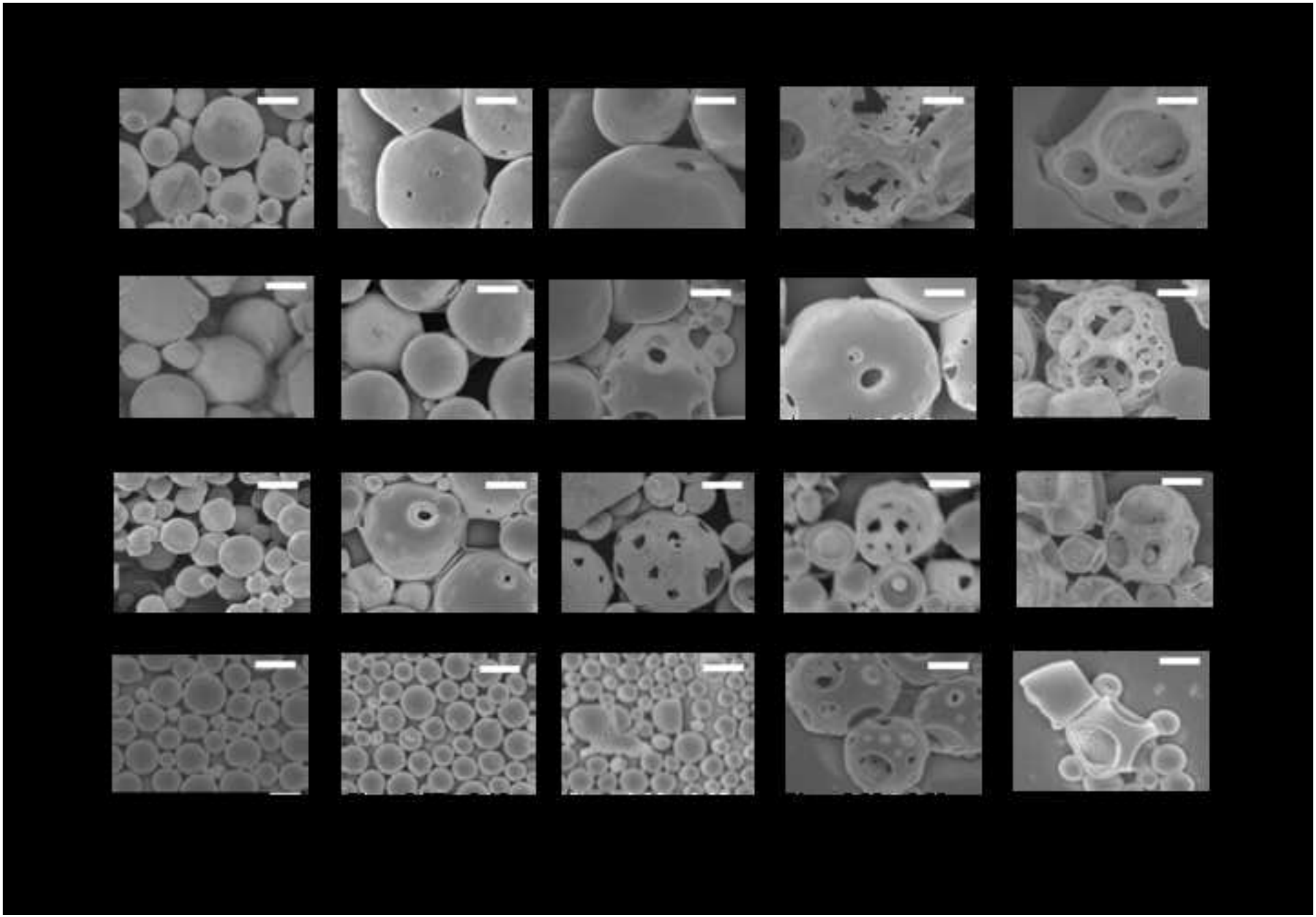

Figure

Click here to access/download;Figure;Figure 4.tiff

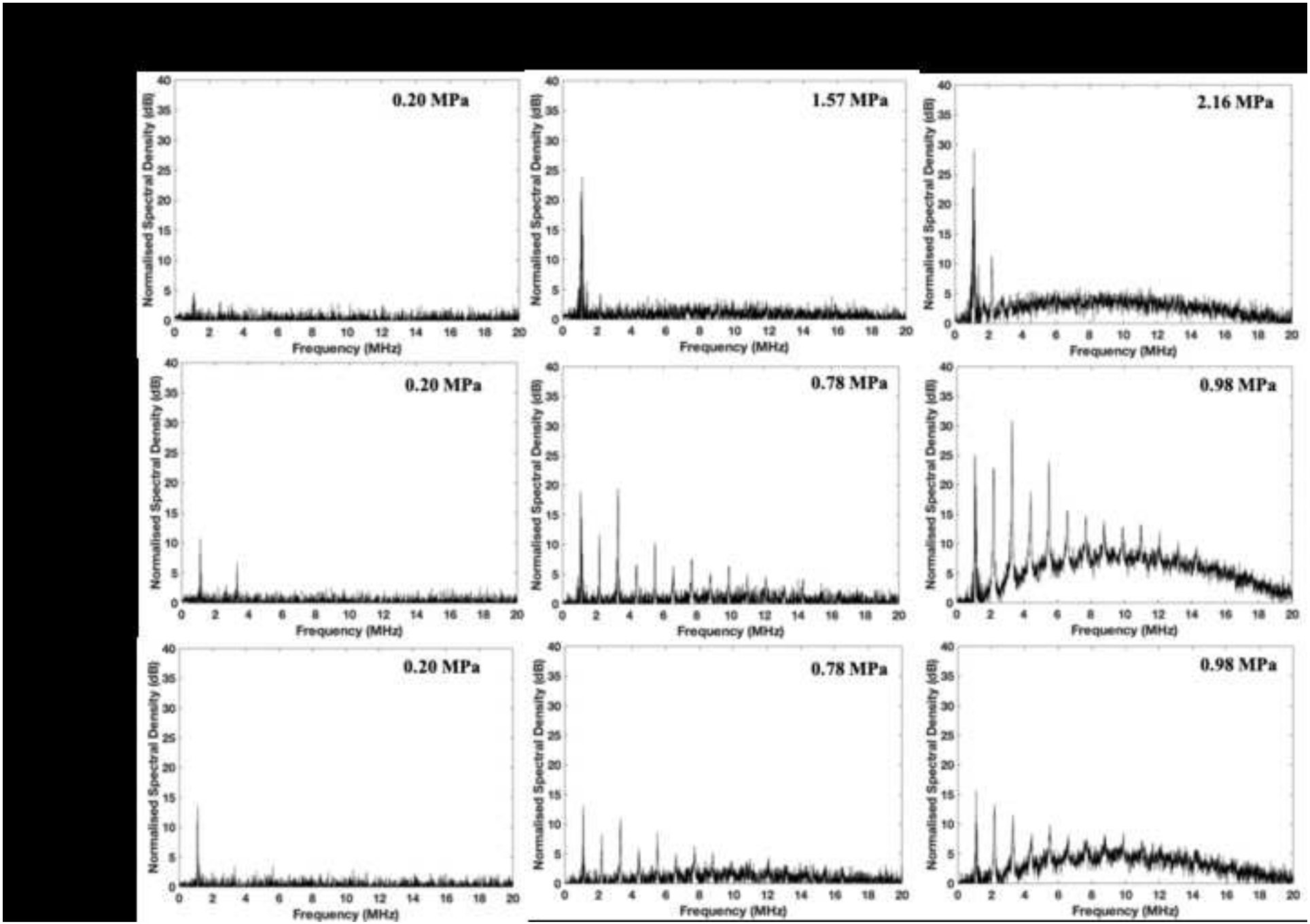

Figure

Click here to access/download;Figure;Figure 5.tiff

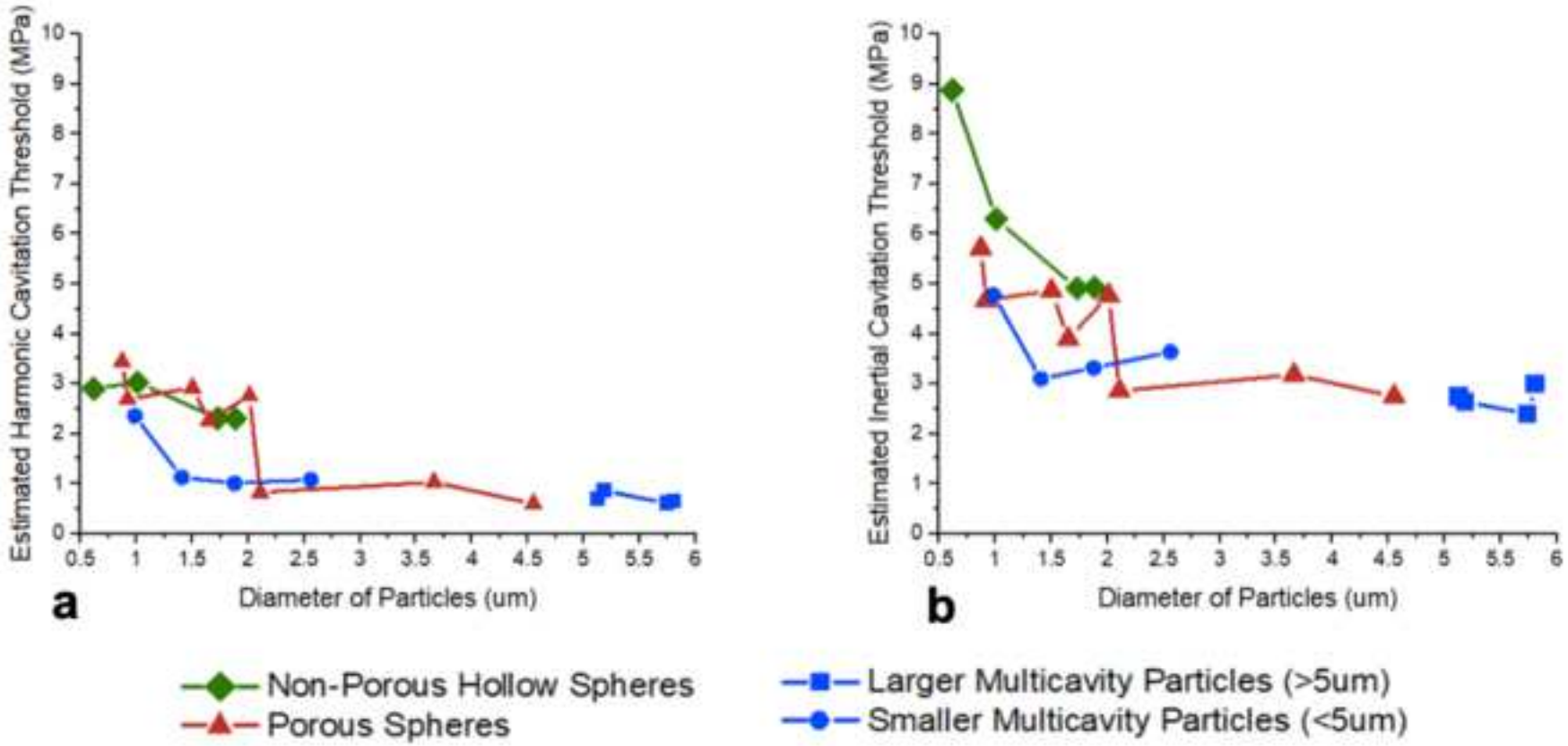

Figure

Click here to access/download;Figure;Figure 6.tiff

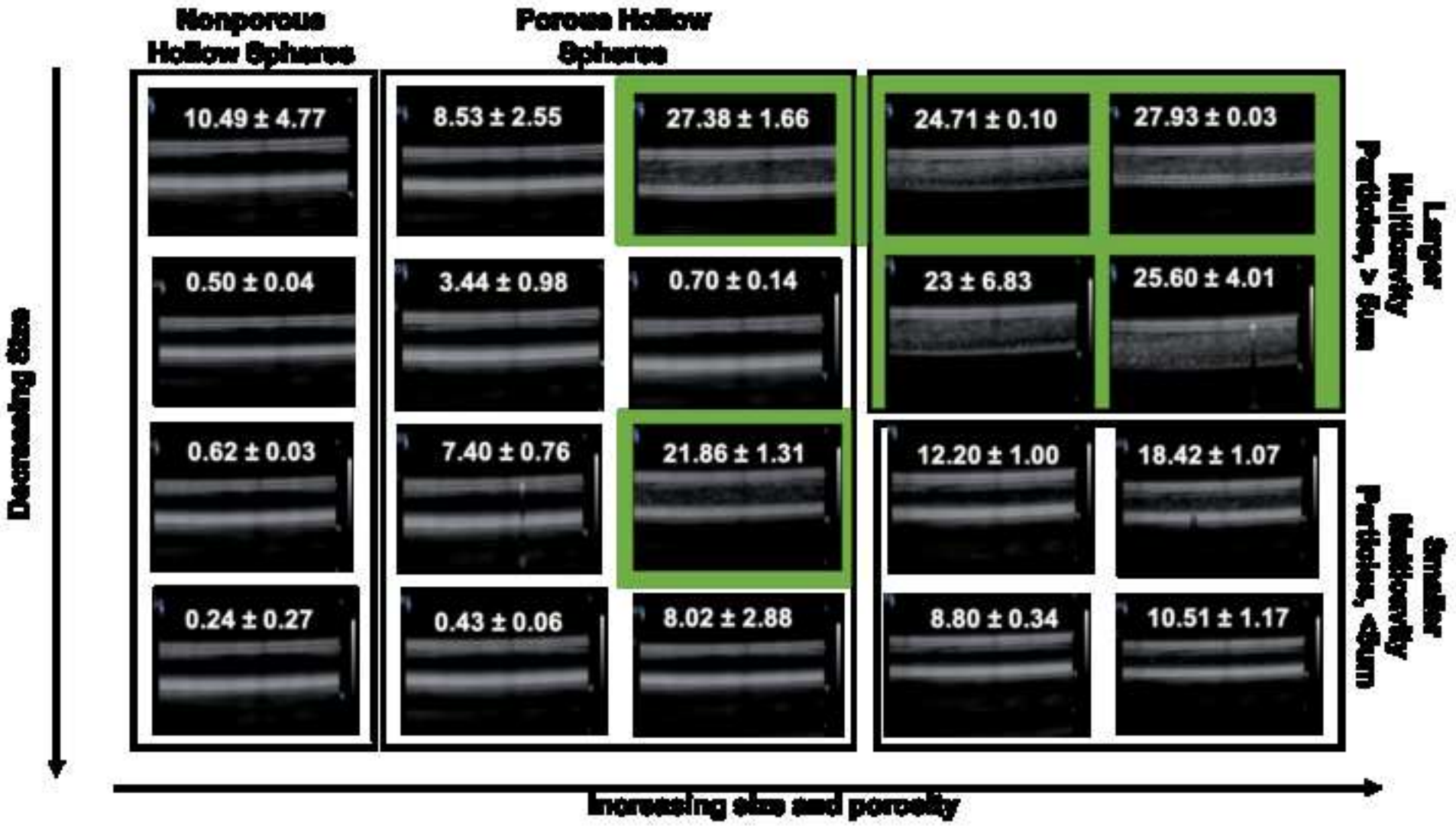

Figure

Click here to access/download;Figure;Figure 7.tiff

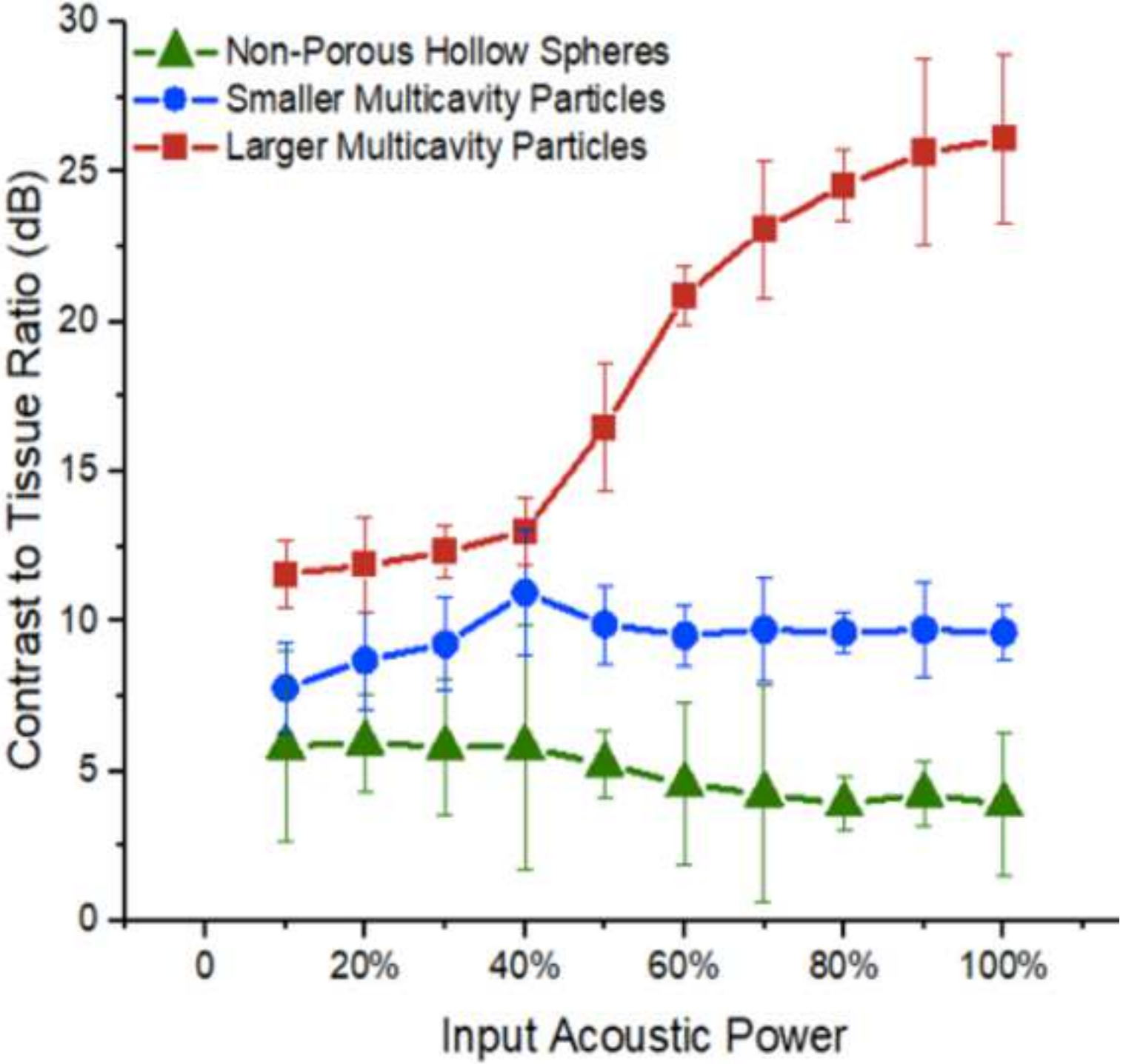

Figure 5

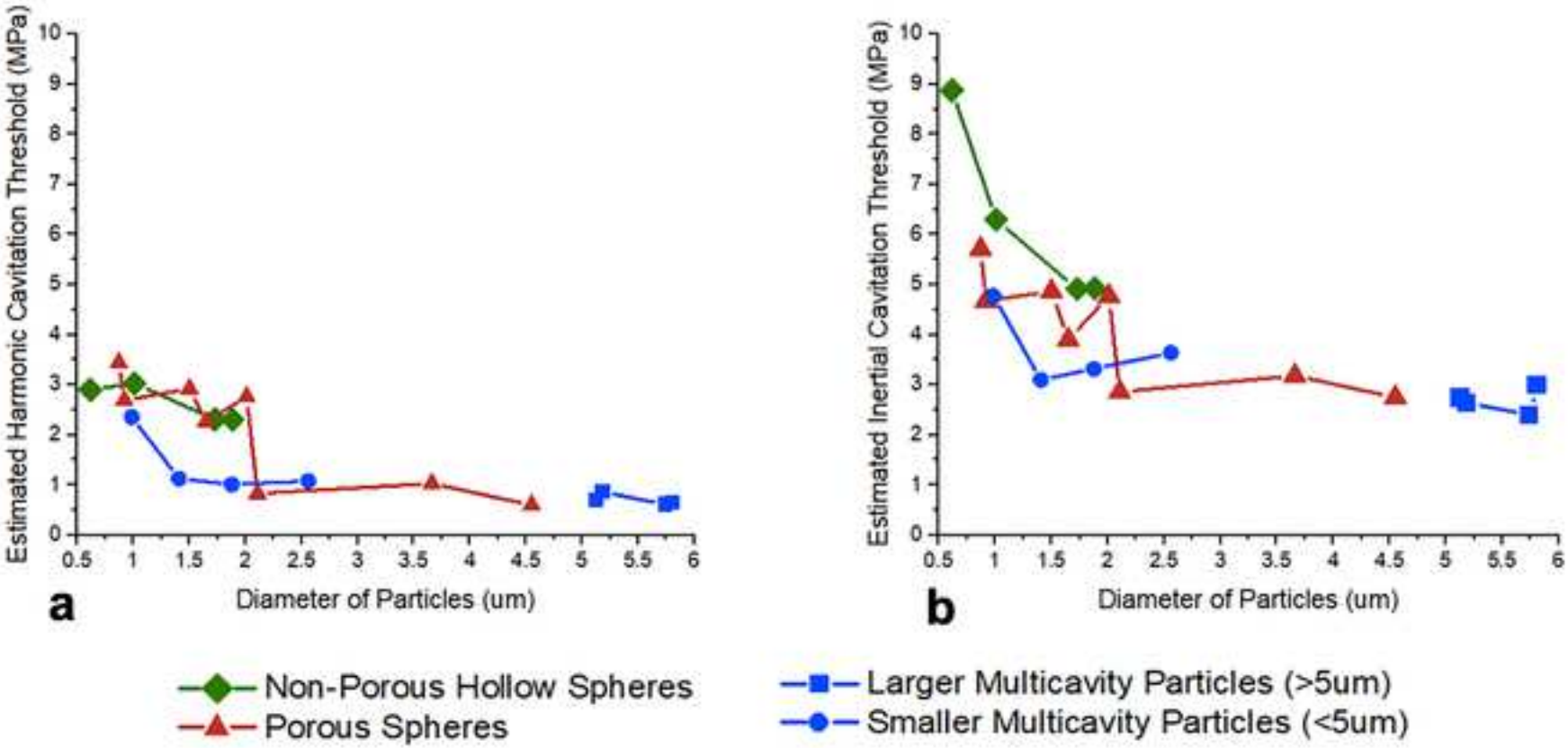

Figure 6

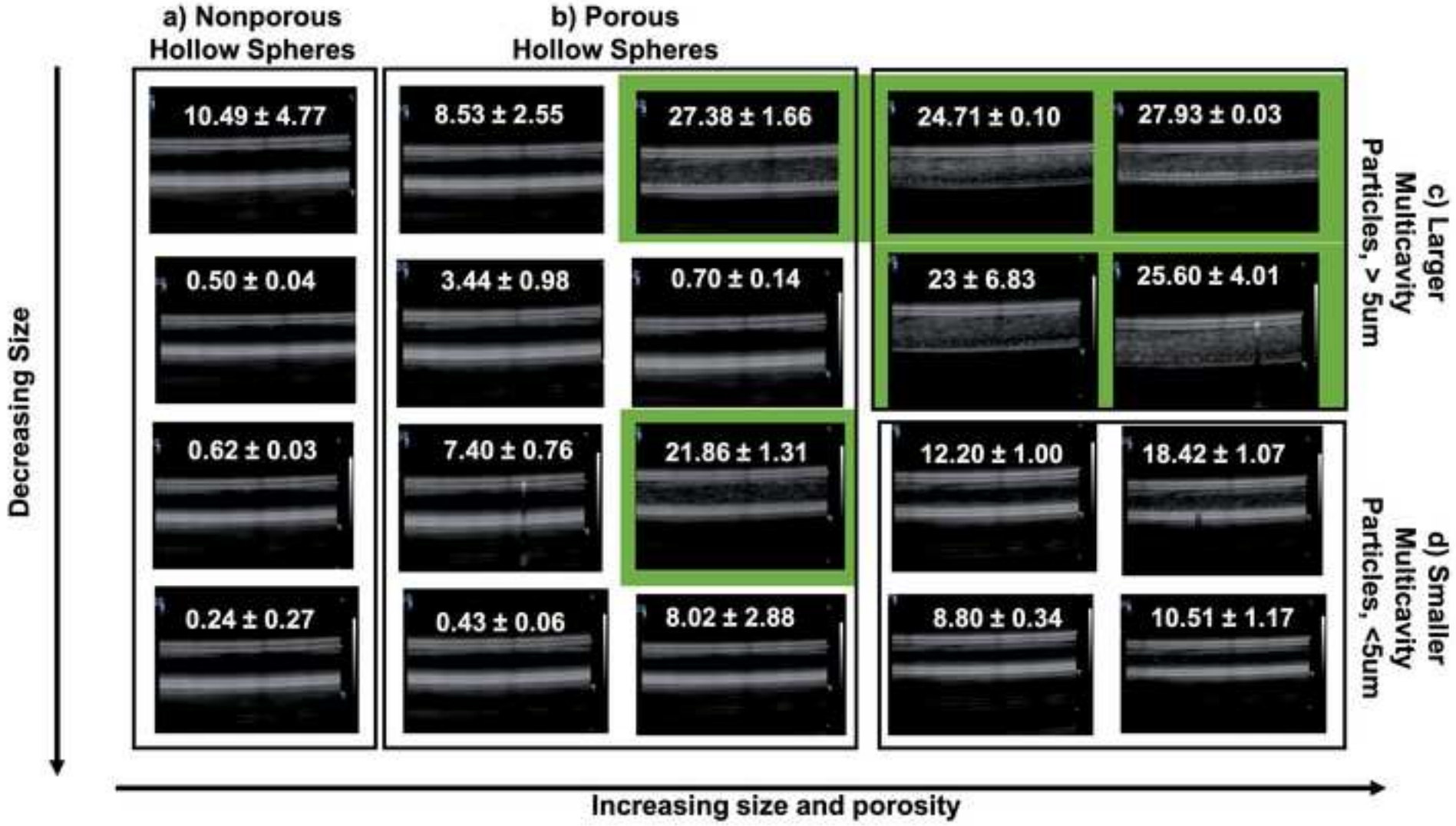

Figure 7

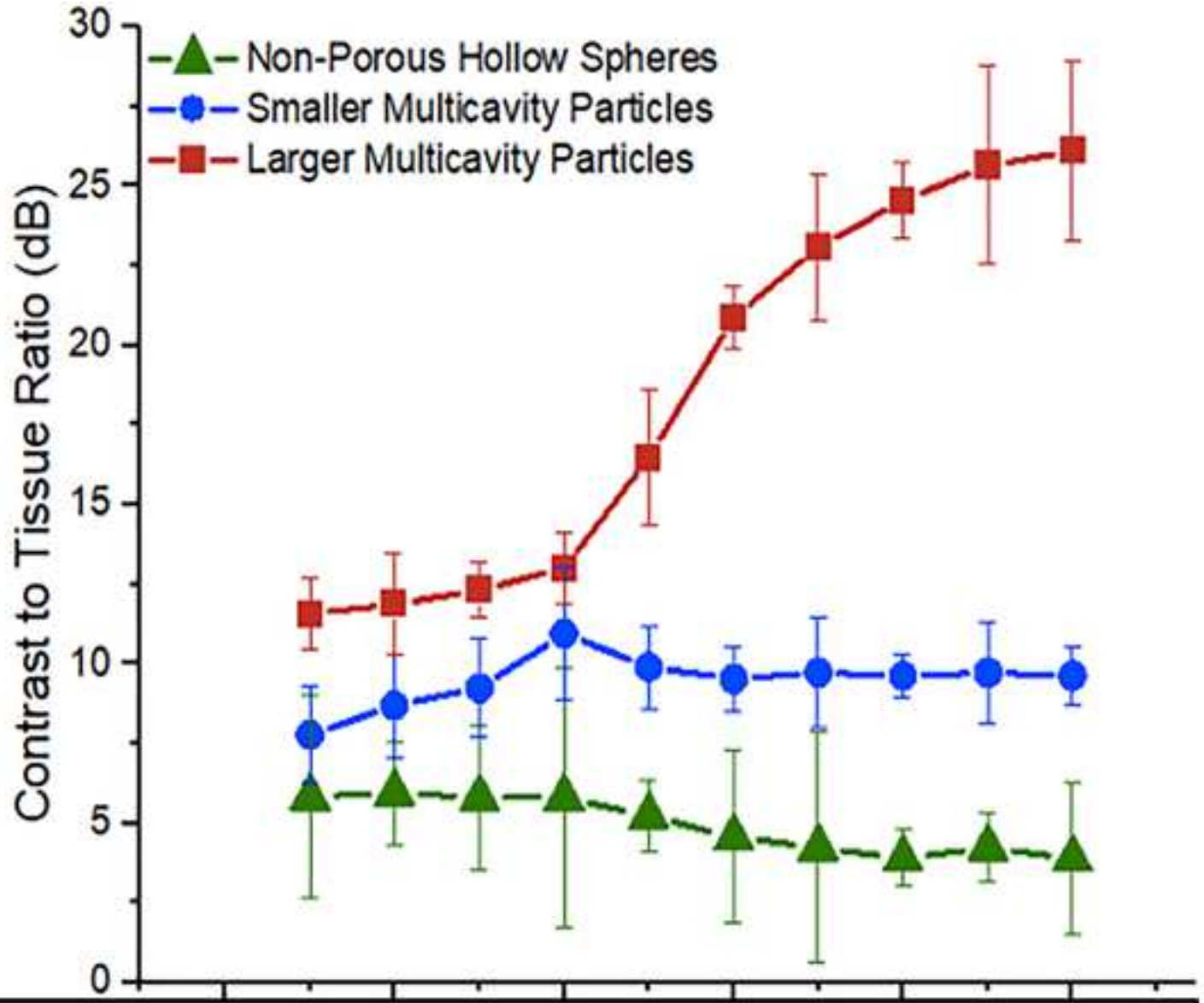

Acoustic Output (%)	0	20%	40%	60%	80%	100%
Peak Negative Pressure (MPa)	0	0.64	1.28	1.92	2.56	3.2
Mechanical Index	0	0.22	0.44	0.66	0.88	1.1

Figure A1

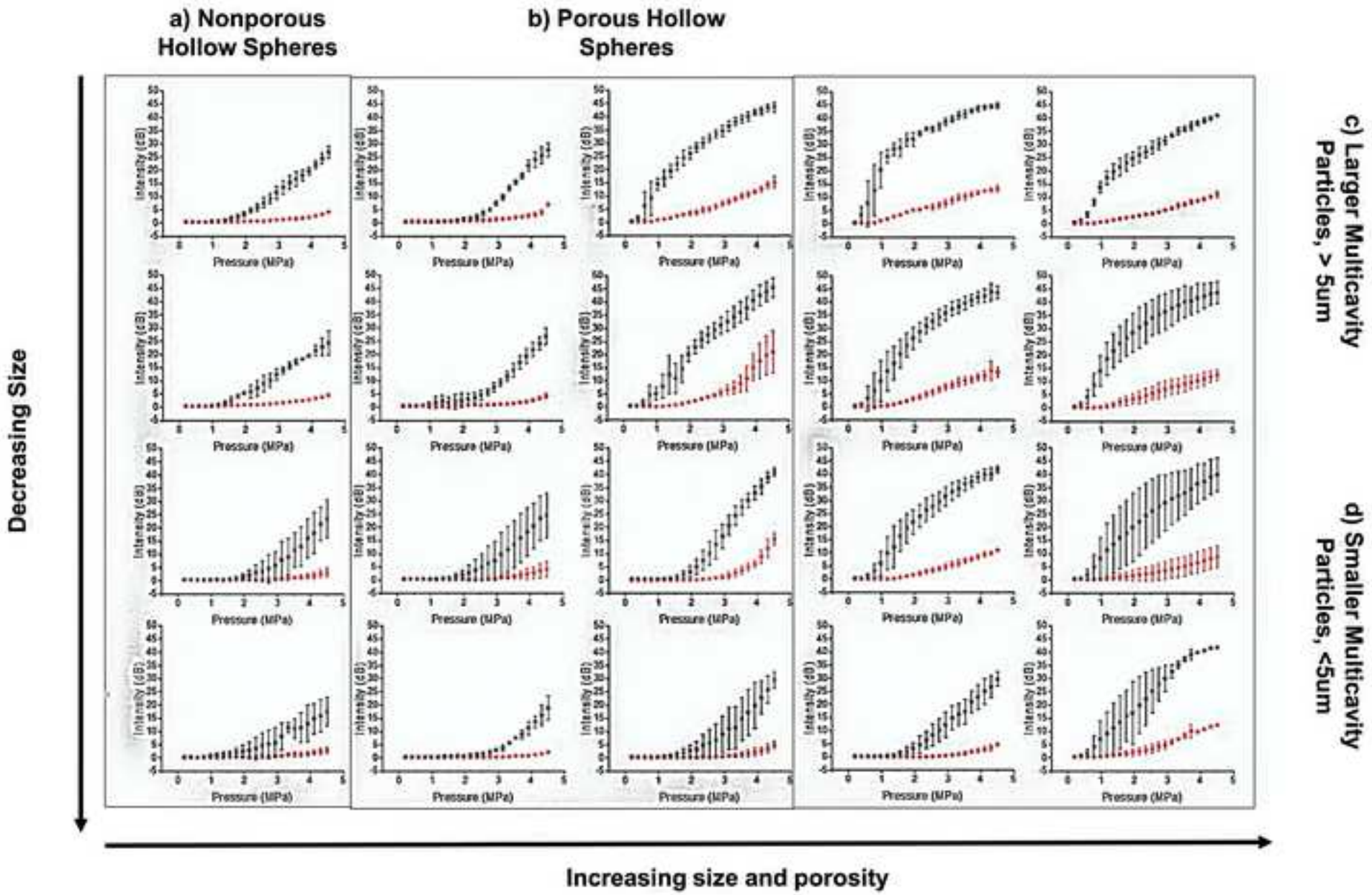

Figure A2

Click here to access/download;Figure;S2 .tif

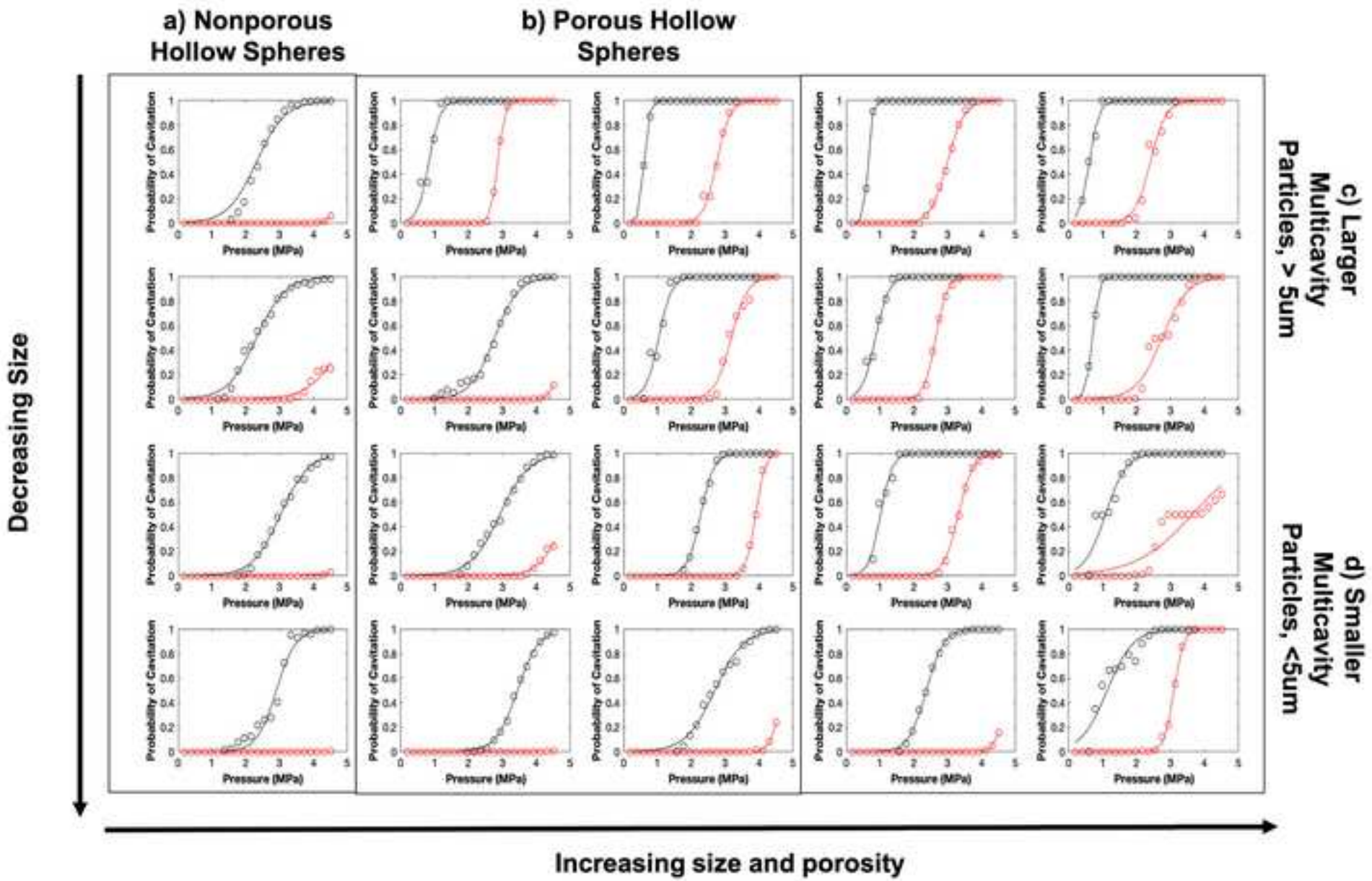

Figure A3

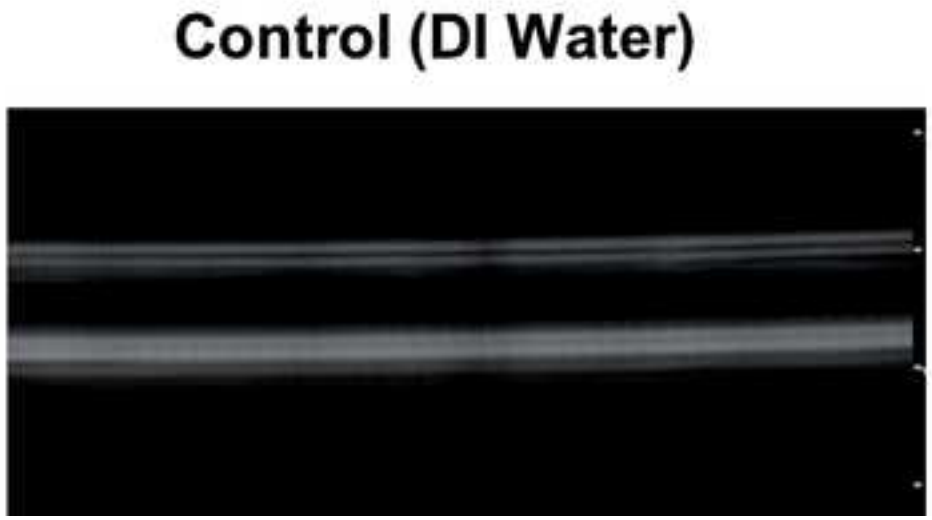

S3.png

Figure 1

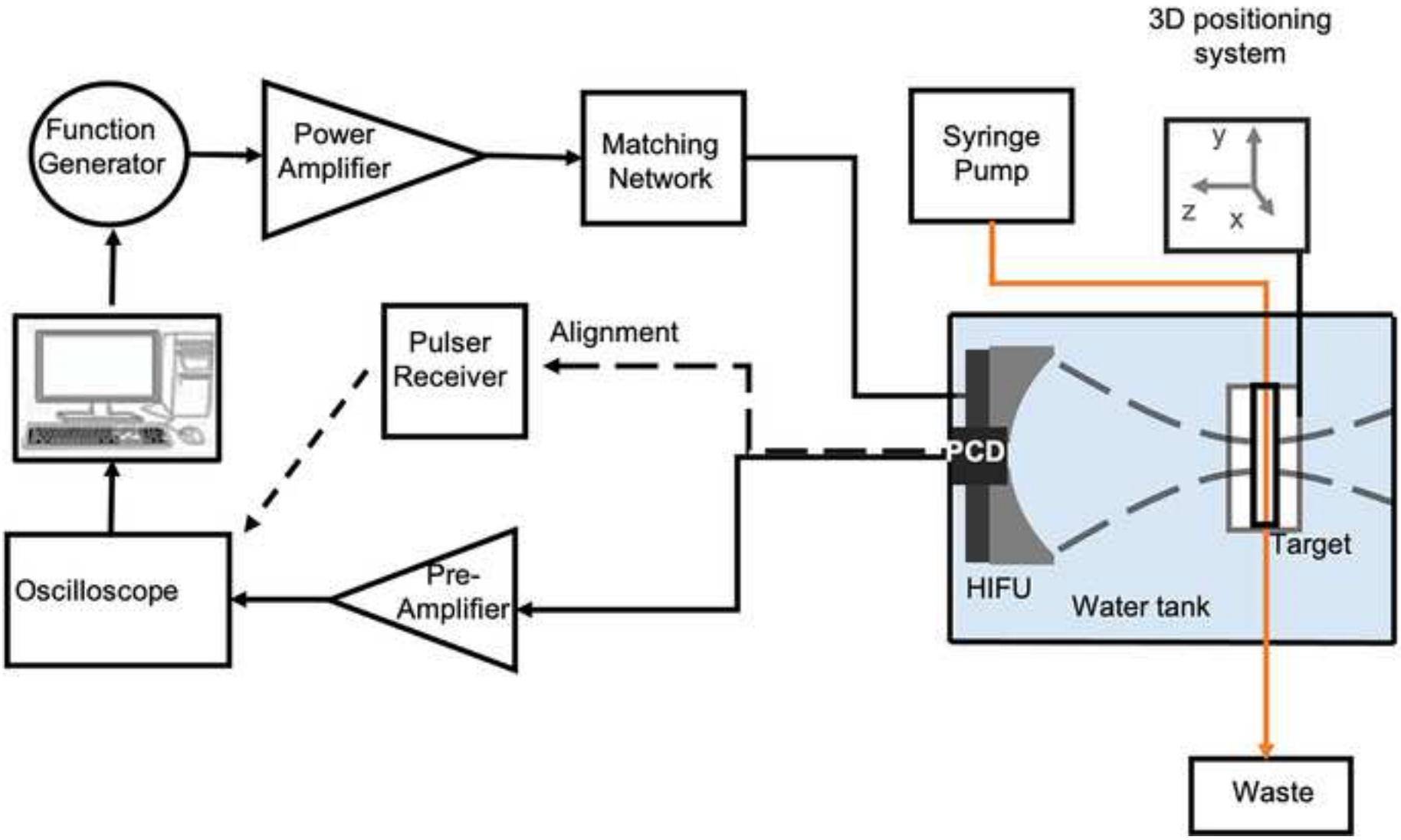

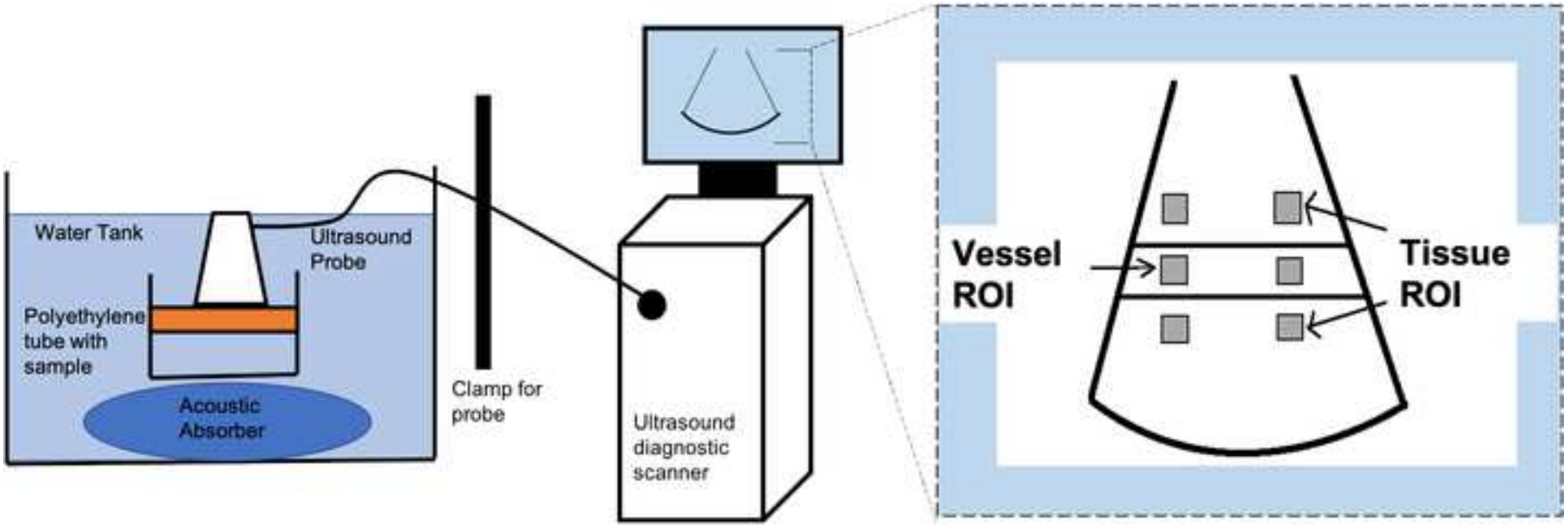

Figure 2.png

Figure 3

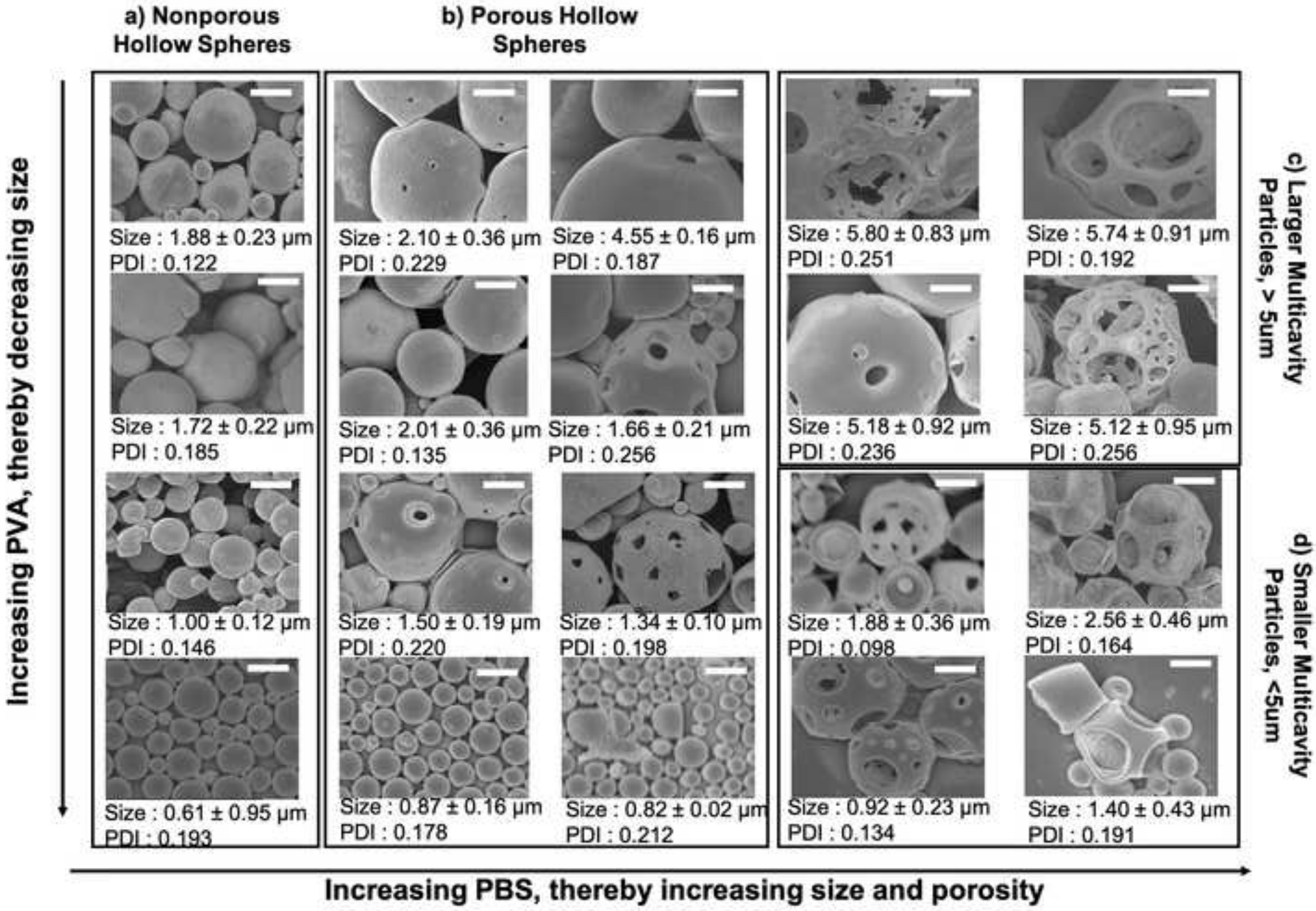

Figure 4